



# Complexes obtained by electrophilic attack on a dinitrogen-derived terminal molybdenum nitride: electronic structure analysis by solid state CP/MAS $^{15}\text{N}$ NMR in combination with DFT calculations

Emma L. Sceats<sup>a</sup>, Joshua S. Figueroa<sup>a</sup>, Christopher C. Cummins<sup>a,\*</sup>, Nikolaus M. Loening<sup>a,b</sup>, Patrick Van der Wel<sup>a,b</sup>, Robert G. Griffin<sup>a,b</sup>

<sup>a</sup> Department of Chemistry, Massachusetts Institute of Technology, 77 Massachusetts Ave., Cambridge, MA 02139, USA

<sup>b</sup> Francis Bitter Magnet Laboratory, Massachusetts Institute of Technology, 77 Massachusetts Ave., Cambridge, MA 02139, USA

Received 25 April 2004; accepted 25 August 2004

Available online 28 October 2004

## Abstract

$^{15}\text{N}$  Solid state CP/MAS NMR spectroscopy has been used to study a dinitrogen-derived terminal nitride of molybdenum,  $^{15}\text{NMo}(\text{N}^i\text{Bu}]\text{Ar})_3$  ( $\text{Ar} = 3,5\text{-(CH}_3)_2\text{C}_6\text{H}_3$ ). A number of Lewis acid adducts, including  $\text{X}_3\text{E-NMo}(\text{N}^i\text{Bu}]\text{Ar})_3$  ( $\text{X} = \text{F}$ ,  $\text{E} = \text{B}$ ;  $\text{X} = \text{Cl}$ ,  $\text{E} = \text{B}$ ,  $\text{Al}$ ,  $\text{Ga}$ ,  $\text{In}$ ;  $\text{X} = \text{Br}$ ,  $\text{E} = \text{Al}$ ;  $\text{X} = \text{I}$ ,  $\text{E} = \text{Al}$ ) and  $\text{Cl}_2\text{E-NMo}(\text{N}^i\text{Bu}]\text{Ar})_3$  ( $\text{E} = \text{Ge}$ ,  $\text{Sn}$ ), were prepared by the combination of  $^{15}\text{NMo}(\text{N}^i\text{Bu}]\text{Ar})_3$  with 1 equiv. of Lewis acid. A series of cationic imido complexes,  $[\text{RNMo}(\text{N}^i\text{Bu}]\text{Ar})_3\text{X}]^+$  was prepared by the reaction of electrophiles,  $\text{RX}$  [ $\text{R} = \text{CH}_3$ ,  $\text{X} = \text{I}$ ;  $\text{R} = \text{PhC}(\text{O})$  or  $\text{Me}_3\text{Si}$ ,  $\text{X} = \text{OTf}$  ( $\text{OTf} = \text{SO}_3\text{CF}_3$ )], with  $\text{NMo}(\text{N}^i\text{Bu}]\text{Ar})_3$ . Deprotonation of  $[\text{CH}_3\text{NMo}(\text{N}^i\text{Bu}]\text{Ar})_3\text{I}]$  by  $\text{LiN}(\text{SiMe}_3)_2$  afforded the ketimide complex  $\text{H}_2\text{CNMo}(\text{N}^i\text{Bu}]\text{Ar})_3$ , which has been shown to undergo a reaction with neat  $\text{CH}_3\text{I}$  to form  $[\text{CH}_3\text{CH}_2\text{NMo}(\text{N}^i\text{Bu}]\text{Ar})_3\text{I}]$ .  $^{15}\text{N}$  solid state CP/MAS NMR spectroscopy was employed in the characterization of each complex. Complementary density functional theory (DFT) studies of  $^{15}\text{NMo}(\text{N}^i\text{Bu}]\text{Ar})_3$  and derivatives enabled a detailed examination of the experimental solid state NMR parameters in terms of electronic structure at the labeled N-atom. Computational analysis demonstrated that significant paramagnetic contributions to the perpendicular components of the chemical shielding tensor ( $\delta_{11}$  and  $\delta_{22}$ ) were responsible for the huge span of the tensor measured for  $^{15}\text{NMo}(\text{N}^i\text{Bu}]\text{Ar})_3$  ( $\Omega = 1187$  ppm). Perturbation of the electronic structure in  $^{15}\text{NMo}(\text{N}^i\text{Bu}]\text{Ar})_3$  upon coordination of a Lewis acid or formation of a cationic imido complex was attributed to stabilization of a  $\sigma$ -symmetric orbital. An upfield shift in the perpendicular components of the chemical shift tensor results from the reduced paramagnetic contribution to these tensor components upon increasing the energy gap between the magnetically coupled occupied and virtual orbitals ( $e_{\text{occ}} - e_{\text{vir}}$ ).  
© 2004 Elsevier Ltd. All rights reserved.

**Keywords:**  $^{15}\text{N}$  solid state NMR; DFT calculations; Molybdenum nitride; Imido complexes; Lewis acids

## 1. Introduction

The use of isotopic labeling of compounds with  $^{15}\text{N}$  to probe their structure and bonding by means of solid state NMR spectroscopy is most commonly seen in bio-

logical systems and organic molecules [1–9]. In contrast, solid state NMR spectroscopy of spin-active nuclei in transition metal complexes has been underutilized [10–16]. The isotropic chemical shift value determined in solution NMR measurements is the most reported spectroscopic parameter, but a wealth of additional information may be gained through the acquisition of solid state NMR spectra [17,18]. The use of  $^{31}\text{P}$  solid state NMR

\* Corresponding author. Tel.: +6174522517; fax: +6172585700.  
E-mail address: [ccummins@mit.edu](mailto:ccummins@mit.edu) (C.C. Cummins).

spectroscopy to probe the structure and bonding in a terminal molybdenum phosphide,  $\text{PMo}(\text{N}[\text{Bu}]\text{Ar})_3$  ( $\text{Ar} = 3,5\text{-(CH}_3)_2\text{C}_6\text{H}_3$ ) was reported previously [19]. The significant anisotropy of the  $^{31}\text{P}$  chemical shift tensor and the enormous paramagnetic deshielding of the  $^{31}\text{P}$  nucleus when the applied field is oriented perpendicular to the Mo–P triple bond were explained in terms of the magnetic coupling of filled and vacant molecular orbitals.

Herein, we extend our study of structure and bonding through the use of solid state NMR spectroscopy to the analogous terminal nitride of molybdenum,  $\text{NMo}(\text{N}[\text{Bu}]\text{Ar})_3$  (**1**) [20]. The splitting of dinitrogen by a three-coordinate molybdenum(III) complex  $\text{Mo}(\text{N}[\text{Bu}]\text{Ar})_3$  was first reported in 1995 [21]. The  $^{15}\text{N}$ -labeled form of **1**,  $^{15}\text{NMo}(\text{N}[\text{Bu}]\text{Ar})_3$  is readily prepared through the use of  $^{15}\text{N}$ -isotopically-enriched dinitrogen gas, thereby making this complex amenable to study by  $^{15}\text{N}$  NMR spectroscopy [22]. The potential of **1** to serve as a platform in N-atom transfer chemistry is currently under investigation in our laboratories. It is of interest to determine what insight solid state NMR spectroscopy can provide into the electronic structure for a molybdenum complex which is activated toward productive removal of the dinitrogen-derived N-atom into an organic product. The synthesis of several derivatives of **1** and subsequent measurement of their  $^{15}\text{N}$  solid state CP/MAS NMR spectra are described.

Complementary density functional theory analyses of **1** and its derivatives were completed utilizing a simplified ligand framework ( $\text{NH}_2$  ligands replacing  $\text{N}[\text{Bu}]\text{Ar}$ ). DFT permits a detailed analysis of experimental solid state NMR parameters ( $\delta_{11}$ ,  $\delta_{22}$  and  $\delta_{33}$ ) via calculation of the absolute shielding tensors [23–27] together with correlation to calculated molecular orbitals. The validity of our analyses of electronic structure may be assessed by comparison of the experimental tensor values with those determined computationally.

## 2. Experimental

### 2.1. General information

Unless stated otherwise, all operations were performed in a vacuum atmospheres drybox under an atmosphere of purified dinitrogen. Diethyl ether, *n*-pentane and dichloromethane were dried and deoxygenated using the method of Grubbs and coworkers [28]. THF was distilled from purple Na/benzophenone ketyl and collected under dinitrogen.  $\text{C}_6\text{D}_6$  and  $\text{CDCl}_3$  were degassed and dried over 4 Å molecular sieves.  $^{15}\text{N}_2$  was purchased from Cambridge Isotope Laboratories (CIL) in 0.1 mL break-seal glass vessels.  $\text{CH}_3\text{I}$  was, freeze–pump–thaw degassed and stored over 4 Å sieves prior to use.  $\text{Mo}(\text{N}[\text{Bu}]\text{Ar})_3$  [20] and benzoyl triflate

[29] were prepared according to the literature procedures. Other chemicals were purified and dried by standard procedures [30] or were used as received. Celite, alumina and 4 Å molecular sieves were dried in vacuo for 36 h at  $\sim 250$  °C. Infrared spectra were recorded on a Bio-Rad 135 Series FT-IR spectrometer.

### 2.2. X-ray crystal structure determinations

The X-ray data collections were carried out on a Siemens Platform three-circle diffractometer mounted with a CCD or APEX CCD detector and outfitted with a low-temperature, nitrogen-stream aperture. The structures were solved by direct methods, with the exception of **1**- $\text{BF}_3$ , which was solved using the Patterson Method, in conjunction with standard difference Fourier techniques and refined by full-matrix least-squares procedures. A summary of crystallographic data is given in Table 1, with full details found in the Supporting Information. The systematic absences in the diffraction data were uniquely consistent with the assigned space groups of  $P2_1$  for **3** and  $P2_13$  for both [**2b**]OTf and [**2d**]I (Flack parameters are 0.01(4),  $-0.01(4)$  and 0.00(3), respectively). No symmetry higher than triclinic was indicated in the diffraction data for **1**- $\text{BF}_3$ . These choices led to chemically sensible and computationally stable refinements. All hydrogen atoms were placed in calculated positions, with the exception of the ketimide protons of **3**, which were located in the electron density map and refined isotropically. The Mo1–N2–C21 unit of [**2d**]I was found to be coincident with a three-fold axis of the  $P2_13$  space group, thus imposing three-site positional disorder in the corresponding methyl group (C22). This disorder was modeled and no hydrogen atoms were generated for methylene carbon C21. Complex [**2c**]OTf crystallized in the centrosymmetric space group  $P2_1/n$  with two-site positional disorder found for the triflate counter ion. This disorder was modeled to 70:30 occupancy over the two sites as indicated by the refinement statistics and resulted in chemically sensible geometries. Isomorphous **1**- $\text{GeCl}_2$  and **1**- $\text{SnCl}_2$  were found to crystallize in the centrosymmetric space group  $P2_1/c$  and both contained two-site positional disorder of the aryl-ring and  $\text{ECl}_2$  residues. Both possible chiral, three-blade propeller orientations of the aryl rings were present and were modeled each with 50% occupancy as indicated by the refinement statistics. Additionally, each aryl-ring orientation corresponded to distinct  $\text{ECl}_2$  orientation and was similarly modeled. Only one orientation of **1**- $\text{GeCl}_2$  and **1**- $\text{SnCl}_2$  is presented in the text. No hydrogen atoms were generated for the aryl rings of **1**- $\text{GeCl}_2$  and **1**- $\text{SnCl}_2$  due to the disorder. All software for diffraction data processing and crystal-structure solution and refinement are contained in the SHELXTL (v6.14) program suite (G. Sheldrick, Bruker XRD, Madison, WI).

Table 1  
Crystallographic data

Compound	1-BF <sub>3</sub>	1-GeCl <sub>2</sub>	1-SnCl <sub>2</sub>	[2b]OTf	[2c]OTf	[2d]I	3
<i>Crystal data</i>							
Empirical formula	C <sub>37</sub> H <sub>56</sub> N <sub>4</sub> MoBCl <sub>2</sub> F <sub>3</sub>	C <sub>36</sub> H <sub>54</sub> N <sub>4</sub> MoGeCl <sub>2</sub>	C <sub>36</sub> H <sub>54</sub> N <sub>4</sub> MoSnCl <sub>2</sub>	C <sub>40</sub> H <sub>63</sub> N <sub>4</sub> MoF <sub>3</sub> SO <sub>3</sub> Si	C <sub>48</sub> H <sub>67</sub> F <sub>3</sub> N <sub>4</sub> MoO <sub>5</sub> S	C <sub>39</sub> H <sub>57</sub> N <sub>4</sub> MoCl <sub>2</sub> I	C <sub>37</sub> H <sub>56</sub> N <sub>4</sub> Mo
Formula weight	791.51	781.54	828.36	861.03	965.06	875.63	652.80
<i>T</i> (K)	193(2)	193(2)	193(2)	193(2)	193(2)	193(2)	193(2)
Crystal system	triclinic	monoclinic	monoclinic	cubic	monoclinic	cubic	monoclinic
Space group	<i>P</i> $\bar{1}$	<i>P</i> 2 <sub>1</sub> / <i>c</i>	<i>P</i> 2 <sub>1</sub> / <i>c</i>	<i>P</i> 2 <sub>1</sub> 3	<i>P</i> 2 <sub>1</sub> / <i>n</i>	<i>P</i> 2 <sub>1</sub> 3	<i>P</i> 2 <sub>1</sub>
<i>Unit cell dimensions</i>							
<i>a</i> (Å)	10.5757(6)	14.803(3)	14.803(3)	16.5578(5)	12.3168(8)	16.3118(6)	11.2145(10)
<i>b</i> (Å)	12.1291(7)	13.711(3)	13.711(3)	16.5578(5)	26.7028(17)	16.3118(6)	11.0462(10)
<i>c</i> (Å)	16.6647(10)	19.132(4)	19.132(4)	16.5578(5)	14.7598(10)	16.3118(6)	14.7723(13)
$\alpha$ (°)	93.3220(10)	90	90	90	90	90	90
$\beta$ (°)	107.3170(10)	90.12(3)	90.12(3)	90	90.4400(10)	90	94.367(2)
$\gamma$ (°)	94.7260(10)	90	90	90	90	90	90
Unit cell volume (Å <sup>3</sup> )	2026.2(2)	3883.0(13)	3883.0(13)	4539.5(2)	4854.3(6)	4340.2(3)	1824.6(3)
<i>Z</i>	2	4	4	4	4	4	2
<i>Data collection</i>							
$\lambda$ (Mo K $\alpha$ ) (Å)	0.71073	0.71073	0.71073	0.71073	0.71073	0.71073	0.71073
$\rho_{\text{calc}}$ (g cm <sup>-3</sup> )	1.297	1.292	1.370	1.260	1.321	1.340	1.188
$\mu$ (mm <sup>-1</sup> )	0.499	1.261	1.131	0.412	0.373	1.166	0.388
Reflections collected	8791	16 135	9171	19 536	20 454	18 731	6978
Independent collections ( <i>R</i> <sub>int</sub> )	5282 (0.0355)	5070 (0.0387)	6358 (0.0308)	1988 (0.0601)	6353 (0.0489)	1907 (0.0620)	4511 (0.0592)
Absorption correction	empirical	none	none	empirical	none	none	empirical
Maximum and minimum transmission	0.3804 and 0.3026	na	na	0.2741 and 0.2191	na	na	0.3092 and 0.2137
<i>Structure refinement</i>							
Refinement method	full-matrix least squares on <i>F</i> <sup>2</sup> was used for all complexes						
Observed reflections [ <i>I</i> > 2 $\sigma$ ( <i>I</i> )]	5282	5070	6358	1988	6353	1907	4511
Number of parameters	433	552	552	160	572	151	387
Number of restraints	0	0	0	0	0	0	1
Goodness-of-fit on <i>F</i> <sup>2</sup>	1.076	1.237	1.217	1.074	1.044	1.068	1.053
<i>R</i> [ <i>I</i> > 2 $\sigma$ ( <i>I</i> )]	0.0488	0.0461	0.0620	0.0269	0.0464	0.0314	0.0406
<i>wR</i> <sub>2</sub>	0.1264	0.1176	0.1602	0.0658	0.1153	0.0744	0.1063

### 2.3. NMR measurements

Solution state  $^1\text{H}$ ,  $^{13}\text{C}$  and  $^{19}\text{F}$  NMR spectra were recorded on a Varian Mercury-300 spectrometer operating at 300 MHz for  $^1\text{H}$ . Solution state  $^{27}\text{Al}$ ,  $^{11}\text{B}$  and  $^{119}\text{Sn}$  NMR spectra were recorded on a Varian INOVA-500 spectrometer operating at 500 MHz for  $^1\text{H}$ .  $^{15}\text{N}$  Solution state NMR spectra were acquired on a Bruker DRX600 spectrometer operating at 600 MHz for  $^1\text{H}$  (60 MHz for  $^{15}\text{N}$ ) and equipped with a triple resonance ( $^1\text{H}/^{13}\text{C}/^{15}\text{N}$ ) probe. All solution NMR chemical shifts are reported in parts per million (ppm) and coupling constants ( $J$ ) in Hertz (Hz).  $^1\text{H}$  and  $^{13}\text{C}$  chemical shifts are reported with respect to the internal solvent ( $\text{C}_6\text{D}_6$ , 7.16 and 128.39;  $\text{THF-d}_8$ , 3.58 and 1.73, 67.57 and 25.37;  $\text{CDCl}_3$ , 7.27 and 77.0).  $^{15}\text{N}$  chemical shifts are referenced to external neat  $\text{CH}_3\text{NO}_2$  ( $\delta = 380.2$  ppm with respect to neat liquid  $\text{NH}_3$  (0.0 ppm)) [22]. Other nuclei were referenced using an external standard, as follows:  $^{19}\text{F}$  spectra were referenced with respect to  $\text{CFCl}_3$  (0.0 ppm);  $^{27}\text{Al}$  spectra were referenced to  $\text{Al}(\text{D}_2\text{O})_6^{3+}$  (1.0 M  $\text{AlCl}_3$  in  $\text{D}_2\text{O}$ ; 0.0 ppm);  $^{11}\text{B}$  spectra were referenced to neat  $\text{BF}_3 \cdot \text{OEt}_2$  (0.0 ppm);  $^{119}\text{Sn}$  spectra were referenced to 0.5 M  $\text{Sn}(\text{CH}_3)_4$  in  $\text{CH}_2\text{Cl}_2$  (0.0 ppm). Solid state  $^{15}\text{N}$  NMR spectra were acquired using a custom-designed spectrometer operating at 501 MHz for  $^1\text{H}$  (50.8 MHz for  $^{15}\text{N}$ ). All spectra were acquired using a triple-resonance ( $^1\text{H}/^{13}\text{C}/^{15}\text{N}$ ) magic-angle spinning (MAS) probe from Chemagnetics (Fort Collins, CO) configured for 4.0 mm zirconium rotors. Spinning frequencies of 3–6.5 kHz were used. The identity of the isotropic peak ( $\delta_{\text{iso}}$ ) was confirmed by measurement of the spectra at several different spinning speeds. Proton–nitrogen cross-polarization (CP) under the Hartmann–Hahn match was used to enhance the sensitivity of all  $^{15}\text{N}$  NMR spectra [31]. Samples were referenced indirectly to the  $^{13}\text{C}$  CP/MAS spectrum of adamantane or directly to the  $^{15}\text{N}$  CP/MAS spectrum of  $\text{NH}_4\text{Cl}$  (acquired prior to each sample acquisition). Both solution and solid state NMR spectra were acquired at 20 °C. For further details of parameters used in the acquisition of solid state NMR spectra refer to the [Supporting Information](#).

### 2.4. Simulation and calculation of solid state NMR spectra

The principal components of the chemical shift tensors were determined experimentally by fitting simulated spectra to the experimental data [32,33] using Simpson [34] (a general simulation program for NMR spectroscopy). The residuals between the simulated spectrum and the experimental spectrum could, in most cases, be reduced to <5%. The Simpson program was also used to calculate spectra based on values of the chemical shift tensor (in ppm) that were calculated using ADF. See the [Supporting Information](#) for further details.

### 2.5. Computational details

Theoretical calculations were carried out using the Amsterdam Density Functional package (version *ADF2002.02*) [35–38]. The Slater-type orbital (STO) basis sets were of triple- $\zeta$  quality augmented with two polarization functions (ADF basis TZ2P). Full electronic configuration was used for all atoms. Relativistic effects were included by virtue of the zero order regular approximation (ZORA) [39–41]. The local density approximation (LDA) by Vosko, Wilk and Nusair (VWN) [42] was used together with the exchange correlation corrections of Becke [43] and Perdew [44] (BP-86).

The  $^{15}\text{N}$  NMR chemical shielding calculations were performed using a multi-step procedure. First, the geometry of the compound of interest was optimized using X-ray parameters as a starting point. The optimized geometry was then subjected to a single-point calculation incorporating spin–orbit effects. The output of this calculation was used as the input for the ADF NMR utility [45].

Values of the absolute shielding tensor, calculated using density functional methods, were converted to referenced chemical shifts ( $\delta$  ppm) using the following equation [46]

$$\delta(\text{S, calc}) = \sigma(\text{N}_2, \text{calc}) - \sigma(\text{S, calc}) + \delta(\text{N}_2, \text{ref}), \quad (1)$$

where  $\delta(\text{S, calc})$  is the calculated chemical shift (ppm) of the compound of interest (S),  $\sigma(\text{N}_2, \text{calc})$  is the calculated absolute shielding tensor for the reference compound ( $\text{N}_2$  gas;  $\sigma(\text{N}_2, \text{calc}) = -80.012$  ppm),  $\sigma(\text{S, calc})$  is the calculated absolute shielding tensor of S and  $\delta(\text{N}_2, \text{ref})$  is the experimental chemical shift (ppm) of the reference compound ( $\text{N}_2$  gas). The NMR shielding ( $\sigma$ ) of  $\text{N}_2$  (with reference to neat nitromethane) = + 74.2 ppm, therefore  $\delta(\text{N}_2, \text{ref}) = 380.2 - 74.2 = 306$  ppm (referenced to liquid  $\text{NH}_3$  at 0 ppm) [47,48].

### 2.6. Synthesis of $^{15}\text{NMo}(\text{N}[\text{tBu}]\text{Ar})_3$ (1)

A 300-mL 3-neck flask fitted with a 0.1 L break-seal flask containing  $^{15}\text{N}_2$  was charged with KH (3.52 g, 88 mmol). THF (50 mL) was added and the slurry was stirred while sparging with argon for 15 min. Stirring was paused and the headspace of the flask was evacuated. Under a static vacuum the break-seal was opened and the slurry was stirred vigorously as the headspace filled with  $^{15}\text{N}_2$ . In a second flask,  $\text{Mo}(\text{N}[\text{tBu}]\text{Ar})_3$  (5.5 g, 8.8 mmol) was dissolved in THF (35 mL) and the solution was stirred while sparging with argon for 10 min. Addition of the  $\text{Mo}(\text{N}[\text{tBu}]\text{Ar})_3$  solution via syringe to the KH/THF slurry afforded a dark orange mixture. Stirring was continued for 24 h after which time the solution was filtered through Celite. Solvent removal in vacuo gave an orange powder, which upon dissolution in pen-

tane and storage at  $-35\text{ }^{\circ}\text{C}$  gave amber crystals of the desired terminal nitride complex,  $^{15}\text{NMo}(\text{N}^t\text{Bu})\text{Ar}_3$  (4.72 g, 7.40 mmol, 84%). This procedure is a modification of previously reported syntheses for complex **1** [20,50,51].

### 2.7. Synthesis of lewis acid adducts **1-LA**

A solution of  $\text{NMo}(\text{N}^t\text{Bu})\text{Ar}_3$  in *n*-pentane (5 mL) was prepared in a 20-mL scintillation vial and chilled to  $-35\text{ }^{\circ}\text{C}$ . In a second vial a solution of the Lewis acid (1 equiv. in 2 mL pentane) was prepared and chilled to  $-35\text{ }^{\circ}\text{C}$ . The Lewis acid solution was added to the  $\text{NMo}(\text{N}^t\text{Bu})\text{Ar}_3$  solution and stirred at room temperature for 1 h. Upon addition of the Lewis acid a yellow solid precipitated from solution. Filtration of the suspension, washing with pentane and subsequent drying under a dynamic vacuum afforded the desired product. Recrystallization from a concentrated  $\text{CH}_2\text{Cl}_2$  solution layered with pentane at  $-35\text{ }^{\circ}\text{C}$  afforded yellow crystals of  $\text{X}_3\text{E-NMo}(\text{N}^t\text{Bu})\text{Ar}_3$ .

Isolated yield of yellow **1-BF<sub>3</sub>·CH<sub>2</sub>Cl<sub>2</sub>** (from 0.115 g of **1**): 0.092 g, 0.130 mmol, 72%. *Anal. Calc.* for  $\text{C}_{36}\text{H}_{54}\text{N}_4\text{MoBF}_3$ : C, 61.19; H, 7.70; N, 7.93. Found: C, 60.94; H, 7.76; N, 7.86%.  $^1\text{H NMR}$  (300 MHz,  $\text{CD}_2\text{Cl}_2$ , 20  $^{\circ}\text{C}$ )  $\delta$ : 6.92 (s, 3 H, *para*), 5.71 (br s, 6 H, *ortho*), 2.15 (s, 18 H,  $\text{ArCH}_3$ ), 1.31 (s, 27 H,  $\text{NC}(\text{CH}_3)_3$ ).  $^{13}\text{C NMR}$  (75.0 MHz,  $\text{CD}_2\text{Cl}_2$ , 20  $^{\circ}\text{C}$ )  $\delta$ : 147.8 (*ipso*), 138.4 (*meta*), 129.9 (*ortho*), 129.1 (*para*), 65.95 ( $\text{NC}(\text{CH}_3)_3$ ), 32.14 ( $\text{NC}(\text{CH}_3)_3$ ), 21.60 ( $\text{ArCH}_3$ ).  $^{19}\text{F NMR}$  (282 MHz,  $\text{CD}_2\text{Cl}_2$ , 20  $^{\circ}\text{C}$ )  $\delta$ : 143.7 (m,  $\text{BF}_3$ ).  $^{11}\text{B NMR}$  (160 MHz,  $\text{CD}_2\text{Cl}_2$ , 20  $^{\circ}\text{C}$ )  $\delta$ : -2.83 (m,  $\text{BF}_3$ ).  $^{15}\text{N-1-BF}_3$ :  $^{11}\text{B NMR}$  (160 MHz,  $\text{CDCl}_3$ , 20  $^{\circ}\text{C}$ )  $\delta$ : -1.72 (br s,  $\nu_{1/2}$  = 49 Hz).  $^{15}\text{N NMR}$  (60 MHz,  $\text{CDCl}_3$ , 20  $^{\circ}\text{C}$ )  $\delta$ : 591.9 (s).

Isolated yield of yellow **1-BCl<sub>3</sub>** (from 0.110 g of **1**): 0.104 g, 0.138 mmol, 80%. *Anal. Calc.* for  $\text{C}_{36}\text{H}_{54}\text{N}_4\text{MoBCl}_3$ : C, 57.20; H, 7.20; N, 7.41. Found: C, 57.11; H, 7.14; N, 7.45%.  $^1\text{H NMR}$  (300 MHz,  $\text{CD}_2\text{Cl}_2$ , 20  $^{\circ}\text{C}$ )  $\delta$ : 6.98 (s, 3 H, *para*), 5.7 (br s, 6 H, *ortho*), 2.19 (s, 18 H,  $\text{ArCH}_3$ ), 1.35 (s, 27 H,  $\text{NC}(\text{CH}_3)_3$ ).  $^{13}\text{C NMR}$  (75.0 MHz,  $\text{CD}_2\text{Cl}_2$ , 20  $^{\circ}\text{C}$ )  $\delta$ : 148.0 (*ipso*), 138.2 (*meta*), 130.8 (*ortho*), 128.6 (*para*), 67.56 ( $\text{NC}(\text{CH}_3)_3$ ), 31.74 ( $\text{NC}(\text{CH}_3)_3$ ), 21.65 ( $\text{ArCH}_3$ ).  $^{11}\text{B NMR}$  (160 MHz,  $\text{CD}_2\text{Cl}_2$ , 20  $^{\circ}\text{C}$ )  $\delta$ : 3.91 (s,  $\nu_{1/2}$  = 16.5 Hz).  $^{15}\text{N-1-BCl}_3$ :  $^{11}\text{B NMR}$  (160 MHz,  $\text{CD}_2\text{Cl}_2$ , 20  $^{\circ}\text{C}$ )  $\delta$ : 4.02 (br s,  $\nu_{1/2}$  = 36.6 Hz).

Isolated yield of yellow **1-AlCl<sub>3</sub>** (from 0.075 g **1**): 0.081 g, 0.104 mmol, 89%. *Anal. Calc.* for  $\text{C}_{36}\text{H}_{54}\text{N}_4\text{MoAlCl}_3$ : C, 55.69; H, 7.01; N, 7.73. Found: C, 55.84; H, 7.11; N, 7.22.  $^1\text{H NMR}$  (300 MHz,  $\text{CD}_2\text{Cl}_2$ , 20  $^{\circ}\text{C}$ )  $\delta$ : 6.95 (s, 3 H, *para*), ~5.6 (br s, 6 H, *ortho*), 2.16 (s, 18 H,  $\text{ArCH}_3$ ), 1.34 (s, 27 H,  $\text{NC}(\text{CH}_3)_3$ ).  $^{13}\text{C NMR}$  (75.0 MHz,  $\text{CD}_2\text{Cl}_2$ , 20  $^{\circ}\text{C}$ )  $\delta$ : 148.2 (*ipso*), 138.4 (*meta*), 130.1 (*ortho*), 128.9 (*para*), 66.38 ( $\text{NC}(\text{CH}_3)_3$ ), 32.40 ( $\text{NC}(\text{CH}_3)_3$ ), 21.61 ( $\text{ArCH}_3$ ).  $^{27}\text{Al NMR}$  (130.1 MHz,

$\text{CD}_2\text{Cl}_2$ , 20  $^{\circ}\text{C}$ )  $\delta$ : 89.30 (s,  $\nu_{1/2}$  = 10 Hz).  $^{15}\text{N-1-AlCl}_3$ :  $^{27}\text{Al NMR}$  (130.1 MHz,  $\text{CD}_2\text{Cl}_2$ , 20  $^{\circ}\text{C}$ )  $\delta$ : 87.76 (m).

Isolated yield of bright yellow **1-AlBr<sub>3</sub>** (from 0.070 g **1**): 0.083 g, 0.092 mmol, 84%. *Anal. Calc.* for  $\text{C}_{36}\text{H}_{54}\text{N}_4\text{MoAlBr}_3$ : C, 47.75; H, 6.01; N, 6.19. Found: C, 47.63; H, 5.88; N, 6.12%.  $^1\text{H NMR}$  (300 MHz,  $\text{CD}_2\text{Cl}_2$ , 20  $^{\circ}\text{C}$ )  $\delta$ : 6.95 (s, 3 H, *para*), 5.70 (br s, 6 H, *ortho*), 2.16 (s, 18 H,  $\text{ArCH}_3$ ), 1.35 (s, 27 H,  $\text{NC}(\text{CH}_3)_3$ ).  $^{13}\text{C NMR}$  (75.0 MHz,  $\text{CD}_2\text{Cl}_2$ , 20  $^{\circ}\text{C}$ )  $\delta$ : 148.2 (*ipso*), 138.3 (*meta*), 130.1 (*ortho*), 129.0 (*para*), 66.66 ( $\text{NC}(\text{CH}_3)_3$ ), 32.50 ( $\text{NC}(\text{CH}_3)_3$ ), 21.62 ( $\text{ArCH}_3$ ).  $^{27}\text{Al NMR}$  (130.1 MHz,  $\text{CH}_2\text{Cl}_2$ , 20  $^{\circ}\text{C}$ )  $\delta$ : 80.17 (br s,  $\nu_{1/2}$  = 85 Hz).  $^{15}\text{N-1-AlBr}_3$ :  $^{27}\text{Al NMR}$  (130.1 MHz,  $\text{CH}_2\text{Cl}_2$ , 20  $^{\circ}\text{C}$ )  $\delta$ : 80.18 (br s,  $\nu_{1/2}$  = 88 Hz).

Isolated yield of yellow **1-AlI<sub>3</sub>** (from 0.100 g **1**): 0.111 g, 0.106 mmol, 68%. *Anal. Calc.* for  $\text{C}_{36}\text{H}_{54}\text{N}_4\text{MoAlI}_3$ : C, 41.16; H, 5.18; N, 5.71. Found: C, 41.16; H, 5.23; N, 5.26%.  $^1\text{H NMR}$  (300 MHz,  $\text{CDCl}_3$ , 20  $^{\circ}\text{C}$ )  $\delta$ : 6.46 (s, 3 H, *para*), 5.47 (br s, 6 H, *ortho*), 1.83 (s, 18 H,  $\text{ArCH}_3$ ), 1.14 (s, 27 H,  $\text{NC}(\text{CH}_3)_3$ ).  $^{13}\text{C NMR}$  (75.0 MHz,  $\text{CDCl}_3$ , 20  $^{\circ}\text{C}$ )  $\delta$ : 136.4 (*meta*), 128.1 (*para*), 32.36 ( $\text{NC}(\text{CH}_3)_3$ ), 20.70 ( $\text{ArCH}_3$ ).  $^{27}\text{Al NMR}$  (130.1 MHz,  $\text{CDCl}_3$ , 20  $^{\circ}\text{C}$ )  $\delta$ : 26.03 (s,  $\nu_{1/2}$  = 226 Hz).  $^{15}\text{N-1-AlI}_3$ :  $^{27}\text{Al NMR}$  (130.1 MHz, THF, 20  $^{\circ}\text{C}$ )  $\delta$ : 24.34 (br s,  $\nu_{1/2}$  = 357 Hz).

Isolated yield of bright yellow **1-GaCl<sub>3</sub>** (from 0.150 g **1**): 0.174 g, 0.214 mmol, 91%. *Anal. Calc.* for  $\text{C}_{36}\text{H}_{54}\text{N}_4\text{MoGaCl}_3$ : C, 53.06; H, 6.68; N, 6.88. Found: C, 53.20; H, 6.62; N, 6.95%.  $^1\text{H NMR}$  (300 MHz,  $\text{CD}_2\text{Cl}_2$ , 20  $^{\circ}\text{C}$ )  $\delta$ : 6.95 (s, 3 H, *para*), 5.62 (br s, 6 H, *ortho*), 2.16 (br s, 18 H,  $\text{ArCH}_3$ ), 1.33 (s, 27 H,  $\text{NC}(\text{CH}_3)_3$ ).  $^{13}\text{C NMR}$  (75.0 MHz,  $\text{CD}_2\text{Cl}_2$ , 20  $^{\circ}\text{C}$ )  $\delta$ : 148.0 (*ipso*), 138.4 (*meta*), 130.1 (*ortho*), 128.9 (*para*), 66.26 ( $\text{NC}(\text{CH}_3)_3$ ), 32.42 ( $\text{NC}(\text{CH}_3)_3$ ), 21.61 ( $\text{ArCH}_3$ ).

Isolated yield of yellow **1-InCl<sub>3</sub>** (from 0.175 g **1**): 0.198 g, 0.230 mmol, 84%. *Anal. Calc.* for  $\text{C}_{36}\text{H}_{54}\text{N}_4\text{MoInCl}_3$ : C, 50.28; H, 6.33; N, 6.52. Found: C, 50.41; H, 6.38; N, 6.67%.  $^1\text{H NMR}$  (300 MHz,  $\text{CDCl}_3/\text{THF}$ , 20  $^{\circ}\text{C}$ )  $\delta$ : 6.59 (s, 3 H, *para*), ~5.6 (br s, 6 H, *ortho*), 1.95 (s, 18 H,  $\text{ArCH}_3$ ), 1.26 (s, 27 H,  $\text{NC}(\text{CH}_3)_3$ ).  $^{13}\text{C NMR}$  (75.0 MHz,  $\text{CDCl}_3/\text{THF}$ , 20  $^{\circ}\text{C}$ )  $\delta$ : 136.7 (*meta*), 128.4 (*ortho*), 32.62 ( $\text{NC}(\text{CH}_3)_3$ ), 21.05 ( $\text{ArCH}_3$ ).

Isolated yield of yellow **1-GeCl<sub>2</sub>** (from 0.075 g **1** and 0.027 g  $\text{GeCl}_2\cdot\text{dioxane}$ ): 0.069 g, 0.079 mmol, 68%. *Anal. Calc.* for  $\text{C}_{36}\text{H}_{54}\text{N}_4\text{MoGeCl}_2$ : C, 54.99; H, 6.92; N, 7.63. Found: C, 55.21; H, 6.91; N, 7.12.  $^1\text{H NMR}$  (300 MHz,  $\text{CDCl}_3$ , 20  $^{\circ}\text{C}$ )  $\delta$ : 6.88 (s, 3 H, *para*), 5.66 (br s, 6 H, *ortho*), 2.15 (s, 18 H,  $\text{ArCH}_3$ ), 1.37 (s, 27 H,  $\text{NC}(\text{CH}_3)_3$ ).  $^{13}\text{C NMR}$  (75.0 MHz,  $\text{CDCl}_3$ , 20  $^{\circ}\text{C}$ )  $\delta$ : 148.4 (*ipso*), 137.7 (*meta*), 129.2 (*ortho*), 128.8 (*para*), 65.11 ( $\text{NC}(\text{CH}_3)_3$ ), 32.66 ( $\text{NC}(\text{CH}_3)_3$ ), 21.56 ( $\text{ArCH}_3$ ).

Isolated yield of yellow **1-SnCl<sub>2</sub>** (from 0.165 g **1**): 0.160 g, 0.193 mmol, 75%. *Anal. Calc.* for  $\text{C}_{36}\text{H}_{54}\text{N}_4\text{MoSnCl}_2$ : C, 51.95; H, 6.54; N, 7.21. Found: C, 52.28; H, 6.53; N, 6.69%.  $^1\text{H NMR}$  (300 MHz,

$\text{CD}_2\text{Cl}_2$ , 20 °C)  $\delta$ : 6.89 (s, 3 H, *para*), 5.68 (br s, 6 H, *ortho*), 2.14 (s, 18 H,  $\text{ArCH}_3$ ), 1.35 (s, 27 H,  $\text{NC}(\text{CH}_3)_3$ ).  $^{13}\text{C}$  NMR (75.0 MHz,  $\text{CD}_2\text{Cl}_2$ , 20 °C)  $\delta$ : 144.6 (*ipso*), 138.1 (*meta*), 129.4 (*ortho*), 129.1 (*para*), 64.60 ( $\text{NC}(\text{CH}_3)_3$ ), 32.93 ( $\text{NC}(\text{CH}_3)_3$ ), 21.59 ( $\text{ArCH}_3$ ).  $^{119}\text{Sn}$  NMR (186 MHz, THF, 20 °C)  $\delta$ : 333 (s,  $\nu_{1/2} = 31$  Hz).  $^{15}\text{N}$ - $\mathbf{1}$ - $\text{SnCl}_2$ :  $^{119}\text{Sn}$  NMR (186 MHz, THF, 20 °C)  $\delta$ : 333 (s,  $\nu_{1/2} = 57$  Hz).

### 2.8. Synthesis of $[\text{CH}_3\text{NMo}(\text{N}^t\text{BuAr})_3]\text{I}$ [ $\mathbf{2a}$ ]I

Crystalline  $\mathbf{1}$  (0.120 g, 0.188 mmol) was dissolved in neat  $\text{CH}_3\text{I}$  (0.8 mL, 12.8 mmol) in a 20 mL vial. The solution was stirred at 25 °C for 20 h after which time removal of excess  $\text{CH}_3\text{I}$  in vacuo and a pentane wash afforded a bright yellow powder in 92% yield (0.137 g, 0.173 mmol).  $^1\text{H}$  NMR (300 MHz,  $\text{CDCl}_3$ , 20 °C)  $\delta$ : 6.99 (s, 3 H, *para*), 5.67 (br s, 6 H, *ortho*), 5.16 (s, 3 H,  $\text{NCH}_3$ ), 2.19 (s, 18 H,  $\text{ArCH}_3$ ), 1.29 (s, 27 H,  $\text{NC}(\text{CH}_3)_3$ ).  $^{13}\text{C}$  NMR (75.0 MHz,  $\text{CDCl}_3$ , 20 °C)  $\delta$ : 145.3 (*ipso*), 138.6 (*meta*), 130.8 (*para*), 128.4 (*ortho*), 68.50 ( $\text{NC}(\text{CH}_3)_3$ ), 65.60 ( $\text{NCH}_3$ ), 32.30 ( $\text{NC}(\text{CH}_3)_3$ ), 21.70 ( $\text{ArCH}_3$ ). NMR data for  $^{15}\text{N}$ - $[\mathbf{2a}]\text{I}$ :  $^1\text{H}$  NMR (300 MHz,  $\text{CDCl}_3$ , 20 °C)  $\delta$ : 5.11 (d,  $^2J_{\text{N-H}} = 3.3$  Hz, 3 H,  $^{15}\text{N}-\text{CH}_3$ ).  $^{15}\text{N}$  NMR (60 MHz,  $\text{CH}_3\text{I}/\text{CDCl}_3$ , 20 °C)  $\delta$ : 462.6. Anal. Calc. for  $\text{C}_{37}\text{H}_{39}\text{D}_{18}\text{N}_4\text{MoI}$ : [49] C, 55.63; H, 7.19; N, 7.01. Found: C, 56.13; H, 7.64; N, 6.53%.

### 2.9. Synthesis of $[(\text{CH}_3)_3\text{Si}-\text{NMo}(\text{N}^t\text{BuAr})_3][\text{SO}_3\text{CF}_3]$ [ $\mathbf{2b}$ ]OTf

A 20-mL scintillation vial was charged with  $\mathbf{1}$  (0.10 g, 0.157 mmol) and  $\text{Et}_2\text{O}$  (2 mL). In a second vial a solution of trimethylsilyl trifluoromethanesulfonate [ $\text{CF}_3\text{SO}_3\text{Si}(\text{CH}_3)_3$ ] (0.174 g, 5 equiv., 0.783 mmol) in  $\text{Et}_2\text{O}$  (1 mL) was prepared. The contents of the two vials were combined and the solution stirred at 25 °C for 10 h. Solvent removal resulted in the isolation of a bright yellow-orange powder; yield 89% (0.120 g, 0.139 mmol). Anal. Calc.: C, 55.75; H, 7.32; N, 6.50. Found: C, 55.54; H, 7.75; N, 6.60%.  $^1\text{H}$  (300 MHz,  $\text{CDCl}_3$ , 20 °C)  $\delta$ : 6.91 (s, 3 H, *para*), 5.62 (br s, 6 H, *ortho*), 2.17 (s, 18 H,  $\text{ArCH}_3$ ), 1.34 (s, 27 H,  $\text{N}(\text{CH}_3)_3$ ), 0.69 (s, 9 H,  $\text{Si}(\text{CH}_3)_3$ ).  $^{13}\text{C}$  NMR (75.0 MHz,  $\text{CDCl}_3$ , 20 °C)  $\delta$ : 147.7 (*ipso*), 137.5 (*meta*), 129.5 (*ortho*), 128.0 (*para*), 66.04 ( $\text{NC}(\text{CH}_3)_3$ ), 32.44 ( $\text{NC}(\text{CH}_3)_3$ ), 21.65 ( $\text{ArCH}_3$ ), 1.94 ( $\text{Si}(\text{CH}_3)_3$ ).  $^{19}\text{F}$  NMR (282 MHz,  $\text{CDCl}_3$ , 20 °C)  $\delta$ : -78.44 (s,  $\text{SO}_3\text{CF}_3$ ).  $^{15}\text{N}$  NMR (60 MHz,  $\text{CDCl}_3$ , 20 °C)  $\delta$ : 537.

### 2.10. Synthesis of $[\text{PhC}(\text{O})\text{NMo}(\text{N}^t\text{BuAr})_3]\text{SO}_3\text{CF}_3$ [ $\mathbf{2c}$ ]OTf

Crystalline  $\mathbf{1}$  (0.200 g, 0.31 mmol) was dissolved in  $\text{CH}_2\text{Cl}_2$  (2 mL) in a 20-mL scintillation vial and chilled to -35 °C. A solution of  $\text{PhC}(\text{O})\text{OTf}$  (0.89 g, 0.37 mmol,

1.2 equiv.) in  $\text{CH}_2\text{Cl}_2$  was prepared and similarly chilled to -35 °C. The  $\text{PhC}(\text{O})\text{OTf}$  solution was added to the stirred solution of  $\text{NMo}(\text{N}^t\text{BuAr})_3$  and an immediate darkening of the solution to a brown-orange color was noted. The solution was stirred at 25 °C for 1 h before concentration of the solution (to ~0.5 mL) and addition of cold  $\text{Et}_2\text{O}$  caused precipitation of a red powder. The solution was filtered and the precipitate washed with pentane to afford a red-orange powder in 72% yield (0.198 g, 0.225 mmol). Material suitable for elemental analysis and crystallographic characterization was prepared by recrystallization from a concentrated THF solution layered with pentane. Anal. Calc.: C, 58.63; H, 6.75; N, 6.36. Found: C, 59.04; H, 6.73; N, 6.20%. IR (KBr plates, THF);  $\nu_{(\text{CO})}$  1668  $\text{cm}^{-1}$ .  $^1\text{H}$  NMR (500 MHz,  $\text{CDCl}_3$ , 20 °C)  $\delta$ : 8.32 (m, 2 H, *meta* Ph), 7.83 (m, 1 H, *para* Ph), 7.77 (m, 2 H, *ortho* Ph), 7.10 (s, 3 H, *para*), 5.74 (br s, 6 H, *ortho*), 2.26 (s, 18 H,  $\text{ArCH}_3$ ), 1.34 (s, 27 H,  $\text{NC}(\text{CH}_3)_3$ ).  $^{13}\text{C}$  NMR (125 MHz,  $\text{CDCl}_3$ , 20 °C)  $\delta$ : 147.7 (*ipso*), 139.1 (*meta*), 136.3 (Ph), 131.5 (Ph), 131.42 (Ph), 130.0 (*para*), 126.8 (*ortho*), 72.0 ( $\text{NC}(\text{CH}_3)_3$ ), 31.8 ( $\text{NC}(\text{CH}_3)_3$ ), 21.7 ( $\text{ArCH}_3$ ).  $^{19}\text{F}$  NMR (282.23 MHz,  $\text{CDCl}_3$ , 20 °C)  $\delta$ : -78.3.

### 2.11. Synthesis of $\text{H}_2\text{CNMo}(\text{N}^t\text{BuAr})_3$ ( $\mathbf{3}$ )

To a chilled suspension of  $[\text{CH}_3\text{NMo}(\text{N}^t\text{BuAr})_3]\text{I}$  (0.098 g, 0.126 mmol) in pentane (5 mL) was added a chilled solution of 1.1 equiv.  $\text{LiN}[(\text{Si}(\text{CH}_3)_2)]_2$  (0.023 g, 0.138 mmol) in pentane (4 mL). Within a few minutes of adding base the yellow suspension turned bright red. The suspension was stirred for 12 h at 25 °C after which time the solution had turned dark purple and no suspended solids were observed. The solution was filtered through Celite and solvent removed in vacuo to yield a dark red-purple solid. Recrystallization from  $\text{Et}_2\text{O}$  yielded dark red crystals 0.051 g (0.077 mmol, 62%). Anal. Calc.: C, 68.017; H, 8.579; N, 8.583. Found: C, 68.22; H, 8.51; N, 8.68%. m.p.: 124–135 °C (dec). IR ( $\text{Et}_2\text{O}$  solution,  $\text{cm}^{-1}$ ): 1600 (m,  $\nu_{\text{NC}}$ ), 1587 (s,  $\nu_{\text{Ar-CH}_3}$ ).  $^1\text{H}$  NMR (300 MHz,  $\text{C}_6\text{D}_6$ , 20 °C)  $\delta$ : 6.69 (s, 3 H, *para*), 6.289 (s, 3 H, *ortho*), 6.287 (s, 3 H, *ortho*), 5.91 (s, 2 H,  $\text{NCH}_2$ ), 2.16 (s, 18 H,  $\text{ArCH}_3$ ), 1.41 (s, 27 H,  $\text{NC}(\text{CH}_3)_3$ ).  $^{13}\text{C}$  NMR (75.0 MHz,  $\text{C}_6\text{D}_6$ , 20 °C);  $\delta$ : 150.2 (*ipso*), 138.9 ( $\text{NCH}_2$ ), 137.4 (*meta*), 129.9 (*ortho*), 127.7 (*para*), 63.1 ( $\text{NC}(\text{CH}_3)_3$ ), 32.8 ( $\text{NC}(\text{CH}_3)_3$ ), 22.1 ( $\text{ArCH}_3$ ).  $^{15}\text{N}$ :  $^1\text{H}$  NMR (300 MHz,  $\text{C}_6\text{D}_6$ , 20 °C)  $\delta$ : 5.90 (d  $^2J_{\text{N-H}} = 1.37$  Hz, 2 H,  $^{15}\text{NCH}_2$ ).  $^{13}\text{C}$  NMR (75.0 MHz,  $\text{C}_6\text{D}_6$ , 20 °C)  $\delta$ : 138.9 (d  $^1J_{\text{N-C}} = 5.78$  Hz,  $^{15}\text{NCH}_2$ ).  $^{15}\text{N}$  NMR (60 MHz,  $\text{C}_6\text{D}_6$ , 20 °C)  $\delta$ : 454.6.

### 2.12. Synthesis of $[\text{CH}_3\text{CH}_2\text{NMo}(\text{N}^t\text{BuAr})_3]\text{I}$ [ $\mathbf{2d}$ ]I

Crystalline  $\text{H}_2\text{CNMo}(\text{N}^t\text{BuAr})_3$  ( $\mathbf{3}$ , 0.074 g, 0.113 mmol) was dissolved in neat  $\text{CH}_3\text{I}$  (0.8 mL) in a 20-mL scintillation vial. The solution was stirred at 25 °C

for 14 h after which time removal of excess  $\text{CH}_3\text{I}$  in vacuo and a pentane wash afforded a bright yellow powder in 96% yield (0.086 g, 0.109 mmol). Recrystallization from a concentrated  $\text{CH}_2\text{Cl}_2$  solution layered with  $\text{Et}_2\text{O}$  afforded yellow crystals of  $[\mathbf{2d}]\text{I} \cdot \text{CH}_2\text{Cl}_2$ .  $^1\text{H}$  NMR (300 MHz,  $\text{CDCl}_3$ , 20 °C)  $\delta$ : 6.98 (s, 3 H, *para*), 5.60 (br s, 6 H, *ortho*), 5.38 (q, 2 H,  $^3J_{\text{HH}}$  7.2 Hz,  $\text{NCH}_2\text{CH}_3$ ), 2.17 (s, 18 H,  $\text{ArCH}_3$ ), 1.95 (t  $^3J_{\text{HH}}$  7.2 Hz, 3 H,  $\text{NCH}_2\text{CH}_3$ ), 1.27 (s, 27 H,  $\text{NC}(\text{CH}_3)_3$ ).  $^{13}\text{C}$  NMR (75.0 MHz,  $\text{CDCl}_3$ , 20 °C)  $\delta$ : 145.9 (*ipso*), 138.6 (*meta*), 130.7 (*para*), 128.3 (*ortho*), 77.6 ( $\text{NCH}_2\text{CH}_3$ ), 68.1 ( $\text{NC}(\text{CH}_3)_3$ ), 32.4 ( $\text{NC}(\text{CH}_3)_3$ ), 21.7 ( $\text{ArCH}_3$ ), 17.5 ( $\text{NCH}_2\text{CH}_3$ ). *Anal.* Calc.: C, 57.43; H, 7.48; N, 7.55. Found: C, 57.52; H, 7.44; N, 7.89%.

### 3. Results and discussion

#### 3.1. Synthesis and characterization

The first reported synthesis of  $\text{NMo}(\text{N}^t\text{BuAr})_3$  (**1**) from  $\text{Mo}(\text{N}^t\text{BuAr})_3$  required a 3 d incubation period at  $-35$  °C during which time  $\text{N}_2$  uptake takes place [20]. Subsequent work focusing on the redox-catalyzed binding and splitting of dinitrogen by  $\text{Mo}(\text{N}^t\text{BuAr})_3$  has led to the development of a more efficient route to the terminal nitride **1** [50]. Most recently, Lewis bases were found to accelerate the uptake of  $\text{N}_2$  by  $\text{Mo}(\text{N}^t\text{BuAr})_3$  enabling its quantitative conversion to **1** within 24 h. Potassium hydride (10 equiv. in THF) was found to be the most efficient base for effecting this conversion (Fig. 1) [51].

Furthermore, the ease of separation of KH from the pentane soluble product (**1**) by filtration makes this route particularly attractive. Complete characterization for complex **1** was reported previously. We will however make note of the  $^{15}\text{N}$  solution NMR shift of **1** (840 ppm) for comparison with values reported in the following discussions. While complex **1** has eluded characterization by single crystal X-ray diffraction, the structure of a related compound,  $\text{NMo}(\text{N}^t\text{BuPh})_3$  [20], is pseudo tetrahedral with the  $\text{Mo}\equiv\text{N}$  bond aligned with a crystallographic  $C_3$  axis.

A number of neutral Lewis acid adducts of formula  $\text{X}_3\text{E}-\text{NMo}(\text{N}^t\text{BuAr})_3$  ( $\text{X} = \text{F}$ ,  $\text{E} = \text{B}$ ;  $\text{X} = \text{Cl}$ ,  $\text{E} = \text{B}$ ,  $\text{Al}$ ,  $\text{Ga}$ ,  $\text{In}$ ;  $\text{X} = \text{Br}$ ,  $\text{E} = \text{Al}$ ;  $\text{X} = \text{I}$ ,  $\text{E} = \text{Al}$ ) and  $\text{Cl}_2\text{E}-\text{NMo}(\text{N}^t\text{BuAr})_3$  ( $\text{E} = \text{Ge}$ ,  $\text{Sn}$ ), were prepared by simple

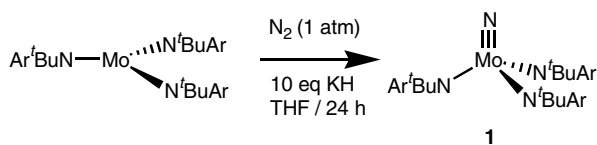


Fig. 1. Formation of complex **1** via the base-catalyzed cleavage of dinitrogen.

combination of **1** with 1 equiv. of Lewis acid (Fig. 2). Yields were generally quite high and in the range of 59–91%. These adducts were typically bright yellow, or sometimes pale orange, exhibiting limited solubility in pentane, benzene and  $\text{Et}_2\text{O}$ . The decomposition of these adducts to starting materials was observed in 0.5–3 h in THF solution at 25 °C.

Infrared spectroscopy yielded little information with regard to the strength of the  $\text{Mo}-\text{N}$  or  $\text{N}-\text{LA}$  ( $\text{LA} = \text{Lewis acid}$ ) interactions as a result of strong absorptions (attributed to the amide ligands) in the relevant regions of the spectrum.

A feature observed in the  $^1\text{H}$  NMR spectrum of all complexes **1-LA** was significant broadening of the  $\sim 5.6$  ppm resonance assigned to the six *ortho* protons of the  $\text{N}^t\text{BuAr}$  ligands. This broadening is attributed to hindered rotation about the  $\text{Mo}-\text{N}_{\text{amide}}$  bond due to increased steric congestion at the metal center.

As expected, the  $^{11}\text{B}$  isotropic chemical shift for **1-BF<sub>3</sub>** ( $-2.8$  ppm) and **1-BCl<sub>3</sub>** (3.9 ppm) showed an upfield shift of each resonance with respect to the uncoordinated Lewis acid ( $\text{BF}_3 = 10.0$  ppm,  $\text{BCl}_3 = 46.5$  ppm).<sup>1</sup> A similar upfield shift of the  $^{27}\text{Al}$  resonance, with respect to the uncoordinated Lewis acid, was observed for the complexes **1-AlCl<sub>3</sub>**, **1-AlBr<sub>3</sub>** and **1-AlI<sub>3</sub>** [52].

The  $^{119}\text{Sn}$  NMR spectrum of **1-SnCl<sub>2</sub>** displayed a broad singlet at 333 ppm, which is shifted downfield of the resonance for  $\text{SnCl}_2$  in THF solution (236 ppm) [53]. The  $^{119}\text{Sn}$  resonance for **1-SnCl<sub>2</sub>** compares with other  $\text{SnCl}_2 \cdot \text{N-donor}$  complexes such as  $\text{SnCl}_2 \cdot \text{pyridine}$  in which the  $^{119}\text{Sn}$  resonance occurs at 295 ppm [54].

In the  $^{27}\text{Al}$ ,  $^{11}\text{B}$  and  $^{119}\text{Sn}$  NMR spectra of  $^{15}\text{N}-\mathbf{1-BX}_3$ ,  $^{15}\text{N}-\mathbf{1-AIX}_3$  and  $^{15}\text{N}-\mathbf{1-SnCl}_2$ , coupling of the two spin active nuclei (e.g.,  $^{15}\text{N}-^{27}\text{Al}$ ) could not be resolved. In each case the resonance for the spin-active Lewis acid center was broadened upon coordination to  $^{15}\text{N}-\mathbf{1}$  (e.g.  $^{11}\text{B}$  NMR:  $^{14}\text{N}-\mathbf{1-BCl}_3$   $\nu_{1/2} = 16.5$  Hz;  $^{15}\text{N}-\mathbf{1-BCl}_3$   $\nu_{1/2} = 36.6$  Hz). Likewise, the  $^{15}\text{N}$  solution NMR spectrum measured for  $^{15}\text{N}-\mathbf{1-BF}_3$  displayed only a broad singlet at 592 ppm. This value is shifted upfield quite considerably (248 ppm) with respect to  $^{15}\text{N}-\mathbf{1}$ .

Crystallographic characterization of **1-BF<sub>3</sub>** confirmed the formation of a  $\sigma$ -bond through donation of the terminal nitride N-lone pair into the vacant p-orbital on the Lewis acidic boron center.<sup>2</sup> The  $\text{N}-\text{B}$  bond distance of 1.609(7) Å is similar to those reported in the literature for other Lewis acid adducts of nitridometal complexes [55–57]. Complex **1-BF<sub>3</sub>** crystallized in the space group  $P\bar{1}$  with the  $\text{B}-\text{F}$  bonds of the Lewis acid staggered with

<sup>1</sup> NMR shifts reported in methylcyclohexane solution; referenced to  $\text{BF}_3 \cdot \text{OEt}_2$  at 0.0 ppm.

<sup>2</sup> See Supporting Information for X-ray crystallographic details and an ORTEP plot of **1-BF<sub>3</sub>**.

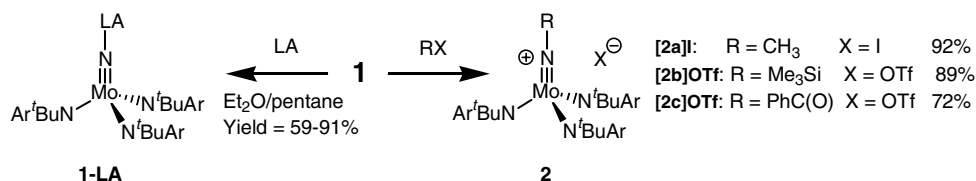


Fig. 2. Syntheses of **1-LA** and the cationic imido complexes **[2a]I**, **[2b]OTf** and **[2c]OTf**.

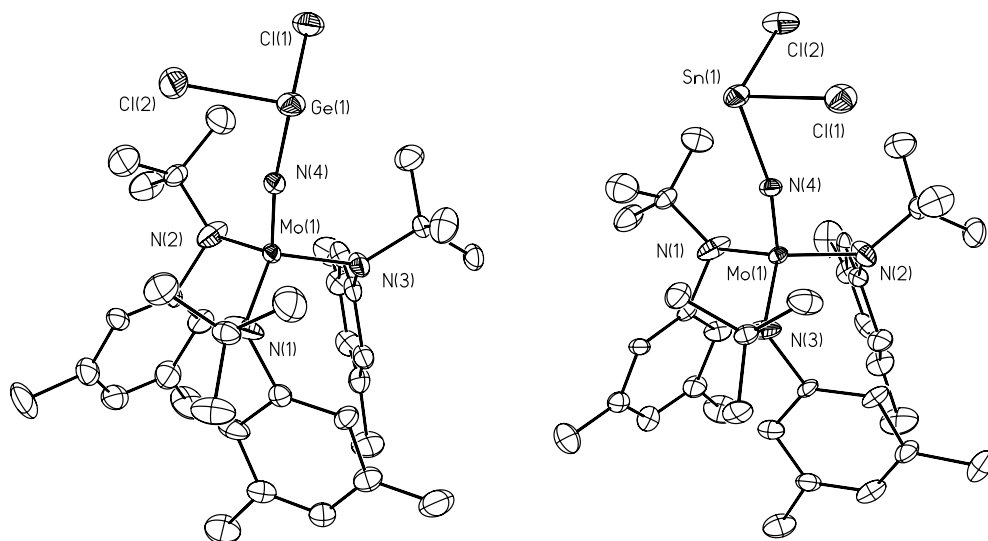


Fig. 3. 35% thermal ellipsoid (ORTEP) representations of **1-GeCl<sub>2</sub>** (left) and **1-SnCl<sub>2</sub>** (right).

respect to the Mo–N<sub>amide</sub> bonds. The Mo≡N bond length (1.678(4) Å) in **1-BF<sub>3</sub>** was identical (to within 3σ) to the Mo≡N bond in NMo(N<sup>t</sup>BuPh)<sub>3</sub> and, as expected, the Mo–N–B bond angle was nearly linear (177.6(4)°).

Complexes **1-GeCl<sub>2</sub>** and **1-SnCl<sub>2</sub>** were found (by X-ray crystallography) to be isomorphous (Fig. 3). To the best of our knowledge, complexes **1-GeCl<sub>2</sub>** and **1-SnCl<sub>2</sub>** represent the first examples of coordination at the terminally bound nitrogen in a nitridometal complex

by a divalent germanium or tin halide [58,59]. Upon addition of GeCl<sub>2</sub>·dioxane or SnCl<sub>2</sub> to **1**, simple Lewis acid adducts analogous to those of the Group 13 **1-LA** complexes were formed. Complexes **1-GeCl<sub>2</sub>** and **1-SnCl<sub>2</sub>** were characterized by Mo≡N bond lengths of ~1.70 Å and N–Ge (or N–Sn) bond lengths typical of single bonds.

Transition-metal imido complexes containing an Mo≡NR bonding motif are well documented in the literature [60,61]. Reaction of **1** with electrophiles, RX

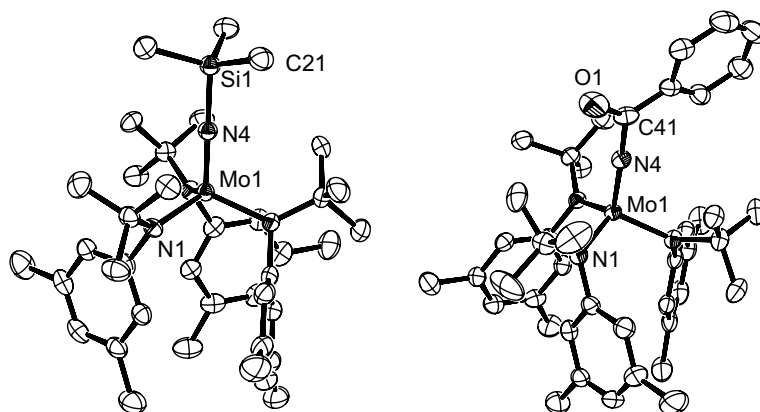


Fig. 4. 50% thermal ellipsoid (ORTEP) representations of cations **[2b]** (left) and **[2c]** (right).

(R = CH<sub>3</sub>, X = I and R = Me<sub>3</sub>Si, X = SO<sub>3</sub>CF<sub>3</sub> = OTf), afforded the imido salts **[2a]I** [49] and **[2b]OTf** as bright yellow, pentane insoluble powders in high yield (92% and 89%, respectively, Fig. 2). In the <sup>1</sup>H NMR spectrum of <sup>15</sup>N-**[2a]I** a two-bond coupling (<sup>2</sup>J<sub>N-H</sub>) of 3.3 Hz was resolved for the methyl protons (<sup>15</sup>N-CH<sub>3</sub>). Solution <sup>15</sup>N{<sup>1</sup>H} NMR spectra for **[2a]I** and **[2b]OTf** displayed resonances at 463 and 537 ppm, respectively.

The imido complex **[2b]OTf** crystallized in the cubic space group *P*2<sub>1</sub>3 (Fig. 4). The Mo–N–Si bond angle is linear as mandated by its alignment with the crystallographic C<sub>3</sub> axis. The Mo≡N bond distance of 1.715(6) Å was lengthened 0.057 Å with respect to the Mo≡N bond distance in **1** while the N–Si bond distance of 1.795(6) Å was slightly longer (~0.08 Å) than might be expected for a single N–Si bond [62]. While complex **[2a]I** has not been structurally characterized, the cation [CH<sub>3</sub>NMo(N<sup>t</sup>BuAr)<sub>3</sub>]<sup>+</sup> **[2a]** is presumably a 4-coordinate monomer related to the trimethylsilylimido cation [(CH<sub>3</sub>)<sub>3</sub>Si–NMo(N<sup>t</sup>BuAr)<sub>3</sub>]<sup>+</sup> **[2b]**.

Reaction of benzoyl triflate (PhC(O)OTf) with **1** in CH<sub>2</sub>Cl<sub>2</sub> enabled isolation of the red-orange benzoylimido complex [PhC(O)NMo(N<sup>t</sup>BuAr)<sub>3</sub>]OTf **[2c]OTf** in 72% yield. There have been very few reports of the use of benzoyl triflate in synthetic inorganic chemistry despite this reagent's obvious utility as a potent electro-

phile [29,63,64]. There are similarly few reports of transition metal complexes containing a benzoylimido moiety i.e., PhC(O)N≡M [65–68]. X-ray crystallographic characterization of **[2c]OTf** showed that the Mo≡N bond is lengthened slightly with respect to the Mo≡N bond in complex **1** (Fig. 4). The N–C bond of 1.422(5) Å is in the range typical for an N–C single bond suggesting that resonance forms involving N–C multiple bond character do not provide added stabilization in this complex.

Dehydrohalogenation of **[2a]I** was achieved using lithium hexamethyldisilazide in pentane (Fig. 5) and resulted in isolation of the purple ketimide complex H<sub>2</sub>CNMo(N<sup>t</sup>BuAr)<sub>3</sub> (**3**). Complex **3** provides a rare example of terminal –NCH<sub>2</sub> complexation [69–72], and represents the first example of such ligation to be structurally characterized (Fig. 6). The ketimide N–C bond distance of 1.300(7) Å is consistent with the presence of an N–C double bond. The Mo–N bond distance of 1.777(4) Å is in the range between that of a Mo–N double bond and that of a Mo–N single bond. This multiple bond character is the result of π-donation from a filled Mo d-orbital into the ketimide π\*(N–C) molecular orbital and in the perpendicular plane, π-donation from the nitrogen lone pair of electrons into a vacant Mo d-orbital. Complex **3** has a distorted tetrahedral geometry

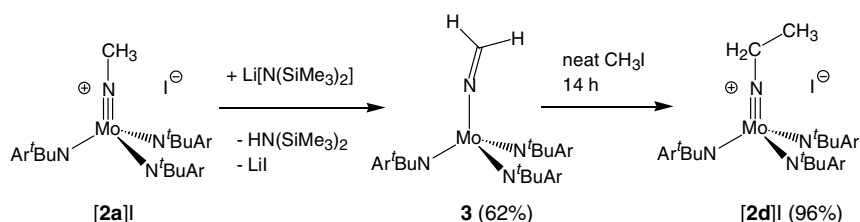


Fig. 5. Dehydrohalogenation of **[2a]I** in the formation of **3** and subsequent reaction with CH<sub>3</sub>I to form **[2d]I**.

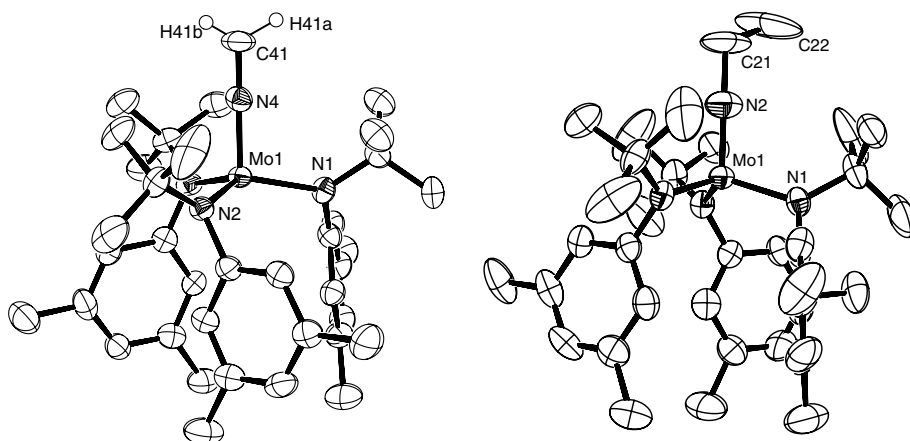


Fig. 6. 50% thermal ellipsoid (ORTEP) representation of **3** (left) and cation **[2d]I** (right).

Table 2

Experimental and calculated  $^{15}\text{N}$  chemical shielding tensors for **1** and derivatives thereof.  $\delta_{iso}$  is the isotropic shift,  $\kappa$  is the span defined as  $\delta_{11} - \delta_{33}$ ;  $\kappa$  is the skew of the shielding tensor defined as  $[3(\delta_{22} - \delta_{iso})/(\delta_{11} - \delta_{33})]$ ;  $\chi^2 = \sum((\text{obs} - \text{calc})^2)/\text{calc}$

Cplx	Model	Principal components of shielding tensor (ppm)												$\chi^2$
		Experimental						Calculated						
		$\delta_{iso}$	$\delta_{11}$	$\delta_{22}$	$\delta_{33}$	$\Omega$	$\kappa$	$\delta_{iso}$	$\delta_{11}$	$\delta_{22}$	$\delta_{33}$	$\Omega$	$\kappa$	
<b>1</b>	<b>1m</b>	833	1229	1229	42	1187	1	795	1137	1137	113	1024	1	
<b>1-BF<sub>3</sub></b>	<b>1m-BF<sub>3</sub></b>	593	836	836	107	729	1	630	878	875	137	741	0.99	12
<b>1-BCl<sub>3</sub></b>	<b>1m-BCl<sub>3</sub></b>	558	773	747	152	621	0.92	562	792	791	102	690	1	31
		555	779	733	154	625	0.85							
<b>1-AlCl<sub>3</sub></b>	<b>1m-AlCl<sub>3</sub></b>	602	864	823	119	745	0.89	624	873	872	128	745	1	4
<b>1-AlBr<sub>3</sub></b>		599	835	835	126	709	1							
<b>1-AlI<sub>3</sub></b>		598	828	828	139	689	1							
		595	810	810	165	645	1							
		591	809	809	156	653	1							
<b>1-GaCl<sub>3</sub></b>	<b>1m-GaCl<sub>3</sub></b>	590	848	813	110	738	0.90	635	886	885	133	753	1	15
<b>1-InCl<sub>3</sub></b>	<b>1m-InCl<sub>3</sub></b>	608	879	874	72	807	0.99	645	902	902	131	771	1	30
		603	846	846	117	729	1							
<b>1-GeCl<sub>2</sub></b>	<b>1m-GeCl<sub>2</sub></b>	643	918	918	93	825	1	660	930	928	123	807	1	8
<b>1-SnCl<sub>2</sub></b>	<b>1m-SnCl<sub>2</sub></b>	666	955	955	89	866	1	669	944	938	125	819	0.99	11
<b>[2a]I</b>	<b>2a-m</b>	457	614	614	143	471	1	463	606	603	182	424	0.99	9
		453	611	611	136	475	1							
		441	594	594	137	457	1							
		436	576	576	156	420	1							
<b>[2b]OTf</b>	<b>2b-m</b>	541	744	716	163	581	0.91	556	758	758	153	605	1	4
<b>[2c]OTf</b>	<b>2c-m</b>	467	701	493	207	494	0.16	507	695	642	183	512	0.79	41
<b>[2d]I</b>	<b>2d-m</b>	460	613	613	153	460	1	486	653	637	168	485	0.93	6
<b>3</b>	<b>3m-C<sub>3</sub></b>	446	591	591	155	436	1	458	600	563	212	388	0.81	18
	<b>3m-C<sub>s</sub></b>							448	570	457	318	252	0.11	125

(average N–Mo–N<sub>amide</sub> bond angle 101.7°) with pseudo-C<sub>3</sub> point symmetry courtesy of the nearly linear (178.0(4)°) Mo–N–C bond axis of the ketimide moiety (which lies along the pseudo-C<sub>3</sub> axis).

The overall sequence leading to complex **3** can be viewed as formal carbene (CH<sub>2</sub>) addition to **1**. Addition of the Group 14 halides GeCl<sub>2</sub> and SnCl<sub>2</sub> to **1** did not give products analogous to **3** (i.e., oxidation Ge/Sn<sup>II</sup> → Ge/Sn<sup>IV</sup> with concomitant formation of a molybdenum(IV) complex Cl<sub>2</sub>E=NMo(N<sup>t</sup>Bu)Ar<sub>3</sub>). This observation is consistent with the increased stability of divalent Group 14 species as the group is descended [73].

Synthesis of the ethylimido complex [CH<sub>3</sub>CH<sub>2</sub>NMo(N<sup>t</sup>Bu)Ar<sub>3</sub>]I [**2d**]I, was achieved by reaction of **3** with CH<sub>3</sub>I (Fig. 5). This reaction demonstrates the nucleophilicity of the ketimide carbon in **3** and is in direct contrast with organic ketimines (RN=CH<sub>2</sub>) which are electrophilic at carbon [74]. Interestingly, we were unable to generate [**2d**] via the reaction of **1** with a suitable source of [CH<sub>3</sub>CH<sub>2</sub>]<sup>+</sup> (e.g., EtI, EtOTf, [Et<sub>3</sub>O]BF<sub>4</sub>). The inability to generate [**2d**] in this way is consistent with the dramatic decrease in rate observed for other nucleophilic substitution reactions (S<sub>N</sub>2) upon increasing the steric bulk at the  $\alpha$ -carbon of the alkyl electrophile (methyl  $\gg$  ethyl > propyl) [75]. Crystallographic characterization of [**2d**]I showed that an N–C single bond (1.457(11) Å) and an Mo–N triple bond (1.708(9) Å) are formed upon the reaction of complex **3** with CH<sub>3</sub>I.

### 3.2. $^{15}\text{N}$ Solid state CP/MAS NMR Spectroscopy of $^{15}\text{NMo}(\text{N}^t\text{Bu})\text{Ar}_3$ (**1**)

Measurement of the  $^{15}\text{N}$  solid state CP/MAS NMR spectrum of  $^{15}\text{NMo}(\text{N}^t\text{Bu})\text{Ar}_3$  (**1**) was carried out in order to probe experimentally the electronic structure at nitrogen. The principal components of the chemical shift tensor can be extracted from the experimental data by simulation of the experimental spectrum or by the analysis of the relative intensities of the spinning sidebands [32,33]. The experimentally measured values of the shift tensor components for **1** and each of its derivatives are presented in Table 2.

The experimental, simulated and DFT calculated  $^{15}\text{N}$  solid state CP/MAS NMR spectra of **1** (calculated spectrum of complex **1m**) are presented in Fig. 7. In the absence of unusual averaging effects, the shift parameter measured in solution for a given complex is equal to the isotropic chemical shift, which is calculated as the average of the principal components of the chemical shift tensor [ $\delta_{iso} = 1/3(\delta_{11} + \delta_{22} + \delta_{33})$ ] [76]. Indeed, the isotropic shift ( $\delta_{iso}$ ) of 833 ppm determined for complex **1** from the solid state NMR spectrum is in close agreement with the  $^{15}\text{N}$  solution NMR shift of 840 ppm. The axial symmetry of complex **1** constrains the orientation of the principal components of the  $^{15}\text{N}$  chemical shift tensor such that the unique axis is aligned along the Mo≡N bond. Our experimental results confirm

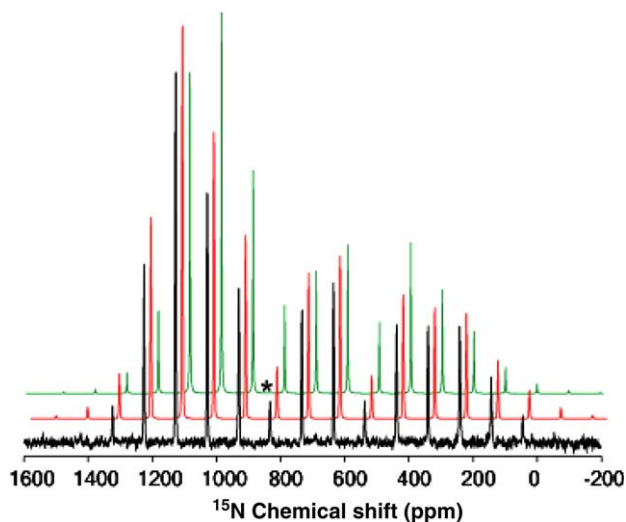


Fig. 7. Experimental (—) and simulated (---)  $^{15}\text{N}$  solid state CP/MAS NMR spectra for complex **1** and DFT calculated (· · ·) NMR spectrum for complex **1m**. The simulated and calculated spectra are offset with respect to the experimental spectrum for clarity. The isotropic peak ( $\delta_{iso}$ ) is indicated by an asterisk.

the axial nature of the chemical shift tensor ( $\delta_{11} = \delta_{22} = 1229$  ppm).

A feature of the spectrum that is immediately obvious is the enormous span ( $\Omega = \delta_{11} - \delta_{33}$ ) of the chemical shift anisotropy (CSA) tensor ( $\Omega = 1187$  ppm). An understanding of the origin of this significant paramagnetic shift at nitrogen, when the external magnetic field is oriented perpendicular to the  $\text{Mo}\equiv\text{N}$  bond, was ascertained by analysis of density functional calculations (see Section 4.1) performed on the model complex  $\text{NMo}(\text{NH}_2)_3$  (**1m**).

### 3.3. $^{15}\text{N}$ solid state CP/MAS NMR spectroscopy of the Lewis acid adducts of **1** (**1-LA**)

The isotropic shift of **1-BF<sub>3</sub>** ( $\delta_{iso} = 593$  ppm) determined from the experimental  $^{15}\text{N}$  solid state NMR spectrum is in excellent agreement with  $\delta_{iso}$  (591 ppm) measured in solution. Complex **1-BF<sub>3</sub>** exhibited an axially symmetric chemical shift tensor wherein  $\delta_{11} = \delta_{22} = 836$  ppm. Solid state  $^{15}\text{N}$  NMR spectra obtained for complexes **1-BCl<sub>3</sub>**, **1-AlCl<sub>3</sub>**, **1-GaCl<sub>3</sub>** and **1-InCl<sub>3</sub>** indicate lower symmetry for the geometries of these complexes ( $\kappa < 1$ ). The isotropic shift for the Lewis acid adducts (**1-LA**) studied was shifted upfield by 167 ppm (**1-SnCl<sub>2</sub>**) to 278 ppm (**1-BCl<sub>3</sub>**) with respect to the terminal nitride (**1**). This upfield shift in the magnitude of  $\delta_{iso}$  can be explained by an increase in the energy gap between occupied frontier molecular orbitals and low-lying virtual molecular orbitals upon coordination of a Lewis acid to the terminally bound N-atom. This information can be extracted from density functional calculations performed on model complexes (**1m-LA**) and is discussed in Section 4.2.

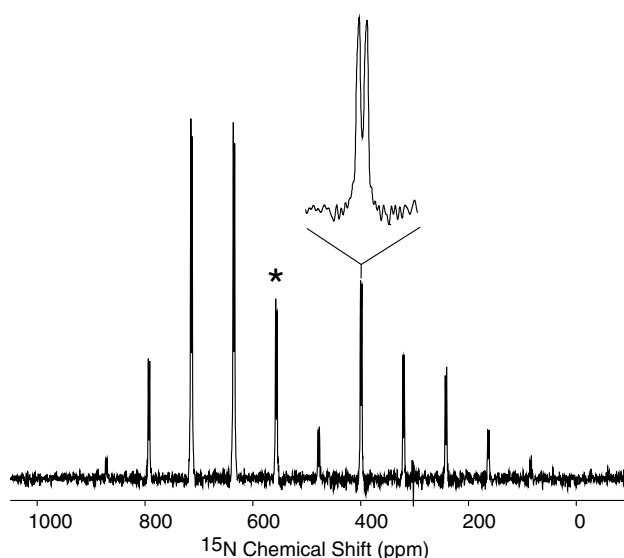


Fig. 8. Experimental  $^{15}\text{N}$  solid state CP/MAS NMR spectrum of **1-BCl<sub>3</sub>**. The expanded portion of the spectrum shows the multiplicity of one of the spinning sidebands. The isotropic peak is marked with an asterisk.

The span ( $\Omega$ ) of the  $^{15}\text{N}$  chemical shift tensor was reduced upon coordination of a Lewis acid, from 1187 ppm in **1** to between 866 ppm (**1-SnCl<sub>2</sub>**) and 621 ppm (**1-BCl<sub>3</sub>**). While the magnitude of the most shielded component  $\delta_{33}$  varied over ca. 90 ppm for **1-LA**, the perpendicular components of the shift tensor,  $\delta_{11}$  and  $\delta_{22}$  (referred to as  $\delta_{\perp}$ ), varied over ca. 180 ppm. Thus, the variation in the span may be attributed primarily to changes in the perpendicular component of the  $^{15}\text{N}$  chemical shielding tensor ( $\delta_{\perp}$ ). Again, this observation can be explained by analysis of the density functional calculations (Section 4.2).

The  $^{15}\text{N}$  solid state NMR spectrum of **1-BCl<sub>3</sub>** displayed multiplicity in the isotropic peak and each of the associated spinning sidebands (Fig. 8).

Two unique sets of data, which differed in the magnitude of the isotropic shift (558 and 555 ppm) and the span of the chemical shift tensor (621 and 625 ppm), were obtained on simulation of the experimental spectrum. Similar multiplicity was observed in the spectra acquired for **1-AlI<sub>3</sub>** and **1-InCl<sub>3</sub>**. This feature could be attributed either to coupling of  $^{15}\text{N}$  with the adjacent spin-active nucleus or structural polymorphism [77–79].

### 3.4. $^{15}\text{N}$ solid state CP/MAS NMR spectroscopy of the imido complexes [**2a**]I, [**2b**]OTf, [**2c**]OTf and [**2d**]I

The axial symmetry of cation [**2a**] was apparent from the tensor components determined by simulation of the  $^{15}\text{N}$  solid state NMR spectrum ( $\delta_{11} = \delta_{22}$ ). The isotropic shift obtained from  $^{15}\text{N}$  solid state NMR measurements (457 ppm) was in excellent agreement with  $\delta_{iso}$  obtained in solution (463 ppm). The spectrum acquired for the

ethylimido complex [2d]I was very similar to that of the methylimido complex [2a]I in terms of the isotropic shift, span and skew of the chemical shift tensor.

Complex [2b]OTf showed unexpected asymmetry in the values of the chemical shift tensor (i.e.,  $\delta_{11} \neq \delta_{22}$ ). Interestingly, the spectrum of [2b]OTf was more reminiscent of those acquired for the Lewis acid adducts (e.g. 1-BCl<sub>3</sub>) in terms of the magnitude of the chemical shift tensors ( $\delta_{nm}$ ) and the span of the spectrum ( $\Omega$ ) than either of the imido complexes [2a]I or [2d]I. Again,  $\delta_{iso}$  obtained for complex [2b]OTf from solid state NMR experiments (541 ppm) was in close agreement with the isotropic shift measured in solution (537 ppm).

The acylimido complex [2c]OTf is unique in the series of imido complexes that are presented in this study for two reasons: (i) significant asymmetry is present in [2c]OTf due to the coordination of the [PhC(O)]<sup>+</sup> electrophile to the terminal nitrogen; (ii) the presence of a carbonyl functional group on the fragment coordinated to N provides an opportunity for resonance stabilization of this imido complex. The asymmetric geometry of complex [2c]OTf was confirmed by the <sup>15</sup>N solid state NMR spectrum for which a rhombic chemical shift tensor ( $\delta_{11} \neq \delta_{22} \neq \delta_{33}$ ) was observed ( $\delta_{11} = 701$  ppm,  $\delta_{22} = 493$  ppm and  $\delta_{33} = 207$  ppm).

The span ( $\Omega$ ) of the <sup>15</sup>N chemical shift tensors for the four imido complexes was in the range of 420–581 ppm, which is smaller than for both 1 ( $\Omega = 1187$  ppm) and the LA adducts (1-LA  $\Omega = 866$ –621 ppm). This reduction in the span could be attributed (in all four complexes) to the reduced magnitude of the most deshielded component of the chemical shift tensor,  $\delta_{11}$ . Again, analysis of density functional calculations performed on model complexes enabled a rationalization of this effect in terms of perturbation of the electronic structure of 1 upon coordination of an electrophile (Section 4.3).

Multiplicity in the isotropic peak and the associated spinning sidebands was observed in the <sup>15</sup>N solid state NMR spectrum of [2a]I.<sup>3</sup> Four isotropic peaks were identified and the span of the chemical shift tensor varied between 420 and 475 ppm. Unlike the Lewis acid adducts (1-LA) for which this multiplicity might be attributed to the adjacent spin-active nucleus, complex [2a]I is thought to display this multiplicity due to structural polymorphism [77–79].

### 3.5. <sup>15</sup>N NMR spectroscopy of H<sub>2</sub>CNMo(N[<sup>t</sup>Bu]Ar)<sub>3</sub> (3)

The experimental <sup>15</sup>N solid state NMR spectrum of 3 displays a number of noteworthy features. First, the principal components of the chemical shift tensor suggest that complex 3 is axially symmetric

( $\delta_{11} = \delta_{22} = 591$  ppm). This symmetry is expected due to the Mo–N multiple bonding in 3 which is attributed to the  $\pi$ -donor/acceptor character of the ketimide (NCH<sub>2</sub>) ligand. The isotropic peak in the <sup>15</sup>N solid state NMR spectrum was in close agreement with that obtained in solution. Complex 3 has the most shielded value of  $\delta_{11}$  with respect to all other complexes measured in this study and a narrow span of the shift tensor ( $\Omega = 436$  ppm).

## 4. Chemical shielding: experimental measurement and computational analysis [76]

The measurement of solid state NMR spectra allows for the experimental determination of the principal components ( $\delta_{11}$ ,  $\delta_{22}$  and  $\delta_{33}$ ) of the chemical shift tensors. To complement our experimental measurements and enable a more complete analysis of these compounds at the electronic level, DFT calculations were performed on model complexes in which the bulky amido ligands N[<sup>t</sup>Bu]Ar were replaced by three NH<sub>2</sub> ligands (for computational expediency). In most cases, the calculated tensors compared favorably with the experimental data<sup>4</sup> thus discussion of the electronic structure based on DFT calculations can be assumed to be valid. A summary of the analysis of the chemical shielding tensors, together with equations relevant to this analysis, are presented here in brief.

The absolute shielding tensor  $\sigma$  (calculated using DFT), is related to the chemical shift tensor  $\delta$

$$\delta = \sigma_{\text{ref}} - \sigma, \quad (2)$$

where  $\sigma_{\text{ref}}$  is the calculated absolute shielding tensor of the reference compound. NMR calculations based on the density functional method have been used to identify the individual contributions to the total shielding tensor made by the diamagnetic ( $\sigma_{\text{dia}}$ ), paramagnetic ( $\sigma_{\text{para}}$ ) and spin orbit ( $\sigma_{\text{so}}$ ) components

$$\sigma_{\text{total}} = \sigma_{\text{dia}} + \sigma_{\text{para}} + \sigma_{\text{so}}. \quad (3)$$

For complexes presented in this study, spin-orbit contributions to the total shielding tensor were included [80,81] but in most cases this contribution was found to be negligible.<sup>5</sup> The diamagnetic contribution is dependent upon the core electron density and acts to reduce the applied magnetic field at the nucleus under observation. In the presence of an applied field  $\sigma_{\text{dia}}$  will generally show insignificant variation in its contribution to the total shielding tensor. The paramagnetic contribution

<sup>3</sup> See Supporting Information for experimental, simulated and calculated <sup>15</sup>N solid state CP/MAS NMR spectra for [2a]I.

<sup>4</sup> Supporting Information: Section 2.15. Plot of the experimental <sup>15</sup>N chemical shift tensor ( $\delta_{11}$ , ppm) vs. Calculated <sup>15</sup>N chemical shift tensor ( $\delta_{11}$ , ppm).

<sup>5</sup> For most of the complexes studied the spin-orbit contribution to the principal components of the chemical shift tensor was <5 ppm.

reinforces the applied field and is determined primarily by magnetic perturbation of the frontier molecular orbitals. Overall,  $\sigma_{para}$  shows the most significant variation in its contribution to the total shielding tensor due to the sensitivity of this term to changes in the electronic environment [82,83]. The paramagnetic contribution to the shielding tensor ( $\sigma_{para}$ ) is proportional to the magnetic coupling of high-lying occupied molecular orbitals with low-lying virtual molecular orbitals ( $M_k$ ) and inversely proportional to the energy difference between these orbitals ( $e_{occ} - e_{vir}$ ). The gauge including atomic orbitals (GIAO) formalism makes it possible to analyze the contributions to the shielding in terms of orbital contributions [84–89]. A molecular orbital analysis of these contributions is contained within the NMR output file of a density functional calculation.<sup>6</sup> This analysis provides a list of the leading contributions to the  $k^{\text{th}}$  component ( $k = 1, 2, 3$ ) of the magnetic field and includes information about the individual pairs of molecular orbitals (which mix in the applied field), the energy difference between these orbitals ( $e_{occ} - e_{vir}$ ) and the magnitude of the coupling ( $M_k$ ). Occasionally, one pair of magnetically coupled molecular orbitals is found to provide the major contribution to the paramagnetic deshielding for each component of the magnetic field ( $k_1, k_2$  and  $k_3$ ).

#### 4.1. Theoretical studies on $^{15}\text{NMo}(\text{N}[\text{tBu}]\text{Ar})_3$ (**1**)

The NMR shift calculation for **1m** predicted an axially symmetric chemical shift tensor in which  $\delta_{11(\text{calc})} = \delta_{22(\text{calc})} = 1137$  ppm. The primary contributions to  $\delta_{11(\text{calc})}$  and  $\delta_{22(\text{calc})}$  resulted from rotational mixing in the presence of an applied field of HOMO–3,  $\sigma(\text{N } p_z\text{–Mo } d_z^2)$  with LUMO,  $\pi^*(\text{N } p_y\text{–Mo } d_{yz})$  and LUMO + 1,  $\pi^*(\text{N } p_x\text{–Mo } d_{xz})$ . There is a relatively small energy gap ( $e_{occ} - e_{vir}$ ) between the filled N  $p_z$  orbital (of  $A$  symmetry in the point group  $C_3$ ), which contains the nitrogen lone pair, and the empty  $\pi^*(\text{Mo–N})$  orbitals (a degenerate  $E$  set in  $C_3$ ). Since the paramagnetic contribution to the chemical shielding tensor is proportional to the coupling between these virtual and occupied orbitals and inversely proportional to the energy gap between them, it follows that the components of the shift tensor ( $\delta_{11}$  and  $\delta_{22}$ ) that are aligned perpendicular to the  $\text{Mo}\equiv\text{N}$  bond will exhibit extreme paramagnetic shifts.

The large paramagnetic contribution to the perpendicular components of the chemical shift tensor ( $\delta_{\perp}$ ) is reminiscent of that observed for related terminal phosphide and carbide complexes [19,90]. In all three examples, the principal contributions to  $\delta_{\perp}$  are the result of mixing in the applied field of a high-lying orbital of  $\sigma$ -

symmetry with a relatively low-lying doubly degenerate  $E$  set of  $\pi$ -symmetry.

For **1** and the derivatives presented in this article, there is a much less significant variation in the magnitude of the most shielded component ( $\delta_{33}$ ) compared to either  $\delta_{11}$  or  $\delta_{22}$ . Where as  $\delta_{11(\text{expt})}$  varies over 653 ppm (1229–576 ppm),  $\delta_{33(\text{expt})}$  varies over a much smaller range of 165 ppm (from 207 to 42 ppm). This can be understood if one considers the chemical shift for a linear molecule. The shift in  $C_{\infty}$  symmetric molecules is dominated by the diamagnetic contribution; the paramagnetic contribution disappears completely along the molecular axis. In **1**, a paramagnetic component to the shift tensor is introduced when the  $C_{\infty}$  symmetry of the  $\text{Mo}\equiv\text{N}$  axis is broken by the addition of ligands to the metal. This paramagnetic component of  $\delta_{33}$  is fairly constant for all of the complexes presented herein.

#### 4.2. Theoretical studies on the Lewis acids adducts of **1** (**1-LA**)

DFT calculations performed on the model complexes **1m-LA** predicted the Lewis acid adducts to be axially symmetric, as evidenced by the calculated skew of the tensor ( $\kappa = 1$  or 0.99 in all cases). Experimental  $^{15}\text{N}$  solid state NMR spectra for **1-BCl<sub>3</sub>**, **1-AlCl<sub>3</sub>** and **1-GaCl<sub>3</sub>**, indicate that the geometry of these complexes is lower than the symmetry to which our DFT calculations converged ( $\kappa < 1$ ). The optimized symmetry of **1m-BF<sub>3</sub>** predicted similar Mo–N and N–B bond lengths to those measured for **1-BF<sub>3</sub>**, however, in the model complex the B–F bonds of the Lewis acid were eclipsed with respect to the Mo–N<sub>amide</sub> bonds. Calculations were performed on model complexes in which either the eclipsed or staggered geometries were enforced in order to gauge the effect of rotation about the N–LA bond on the  $^{15}\text{N}$  chemical shift. In general, calculations for the eclipsed and staggered geometries predicted very similar values of the principal components of the  $^{15}\text{N}$  chemical shift tensor.

In each of the model Lewis acid adducts (**1m-LA**) the principal contributions to  $\delta_{\perp}$  resulted from rotational mixing in the applied field of an occupied  $\sigma$ -orbital with a vacant  $\pi^*(\text{Mo–N})$  orbital. The occupied orbital is characterized by significant N  $p_z$  character, involved in donation of the N-lone pair into the vacant orbital on the Lewis acid's central atom. For example, analysis of the DFT calculation performed on **1m-BCl<sub>3</sub>** shows that the principal contributions to  $\delta_{11}$  and  $\delta_{22}$  are provided by mixing in the applied field of HOMO – 4,  $\sigma(\text{N } p_z\text{–B } p_z)$  with LUMO,  $\pi^*(\text{N } p_y\text{–Mo } d_{yz})$  and LUMO + 1,  $\pi^*(\text{N } p_x\text{–Mo } d_{xz})$ , respectively.<sup>7</sup>

<sup>6</sup> Supporting Information: Section 2.13. Representative input and output files of an NMR calculation.

<sup>7</sup> See Supporting Information 2.17 for selected (calculated) orbitals of **1m-BCl<sub>3</sub>**.

The energy gap ( $e_{\text{occ}} - e_{\text{vir}}$ ) between the occupied  $\sigma(\text{N-LA})$  bonding orbital and the vacant  $\pi(\text{Mo-N})$  orbitals was found to depend principally on the extent to which Lewis acid coordination to the terminal N-atom lowers the energy of the  $\sigma(\text{N } p_z\text{-LA } sp)$  orbital. In **1**, the occupied ( $\text{N } p_z$ ) orbital contains a non-bonding lone pair of electrons and is at a relatively high energy. Formation of a  $\sigma$ -bond to the Lewis acid lowers the energy of this orbital thereby increasing the energy gap between the magnetically coupled virtual and occupied orbitals ( $e_{\text{occ}} - e_{\text{vir}}$ ). This in turn reduces the paramagnetic contribution to the perpendicular component of the chemical shift tensor resulting in more upfield shifted values of  $\delta_{11}$  and  $\delta_{22}$ .

Complex **1m-BCl<sub>3</sub>** has a smaller energy gap ( $e_{\text{occ}} - e_{\text{vir}} = 3.65$  eV) compared to **1m-BF<sub>3</sub>** ( $e_{\text{occ}} - e_{\text{vir}} = 5.06$  eV) but also a reduced paramagnetic contribution to the chemical shift, as evidenced by the more upfield shift of  $\delta_{11(\text{calc})}$ . This apparently anomalous result can be explained if one accounts for the proportional relationship between the paramagnetic contribution to the chemical shift and the magnitude of the coupling ( $M_k$ ) of occupied and virtual molecular orbitals in the presence of an applied magnetic field. Analysis of the DFT calculations for these two complexes shows that  $M_k$  in **1m-BF<sub>3</sub>** (0.438) is more than twice that calculated for **1m-BCl<sub>3</sub>** (0.206). This suggests that a much larger contribution to the paramagnetic term is made by N-based orbitals in **1m-BF<sub>3</sub>** compared to **1m-BCl<sub>3</sub>**.

#### 4.3. Theoretical studies on the imido cations [**2a-m**], [**2b-m**], [**2c-m**] and [**2d-m**]

Calculations performed on the model cation [**2a-m**] predicted an axially symmetric spectrum ( $\delta_{11(\text{calc})} \approx \delta_{22(\text{calc})}$ ), which was in close agreement with the data obtained experimentally for this complex. Upon formation of an N–C single bond in cation [**2a-m**] there is a more significant lowering in energy of the  $\sigma(\text{N-C})$  molecular orbital compared to that observed for the Lewis acid adducts (**1-LA**) discussed previously. This can be attributed to the build up of positive charge on the complex and the increased bond strength of the  $\sigma(\text{N-C})$  bond compared to the  $\sigma(\text{N-LA})$  bond. All four of the imido complexes exhibit a significant energy gap ( $e_{\text{occ}} - e_{\text{vir}}$ ) between the filled  $\sigma(\text{N-E})$  orbital to the lowest lying unoccupied orbitals of  $\pi$ -symmetry. The stabilization of this  $\sigma(\text{N-E})$  bonding orbital prohibits its participation in mixing interactions that supplement the paramagnetic contribution to the chemical shift tensor. For the model cation [**2a-m**] the principal contributions to  $\delta_{\perp}$  result from rotational mixing in the applied field of two occupied orbitals of  $\pi$ -symmetry (a doubly degenerate  $E$  set) with a vacant orbital of  $\sigma$ -symmetry ( $A$  symmetry in  $C_3$ ). Analysis of the DFT calculation performed on [**2a-m**] shows that the principal contribu-

tions to  $\delta_{11}$  and  $\delta_{22}$  ( $\delta_{11(\text{calc})} = 606$  ppm,  $\delta_{22(\text{calc})} = 603$  ppm) are provided by mixing in the applied field of HOMO–2,  $\pi(\text{Mo } d_{xz}\text{-N } p_x)$  and HOMO–3,  $\pi(\text{Mo } d_{yz}\text{-N } p_y)$  with LUMO + 2,  $\sigma^*(\text{N } p_z\text{-C } p_z)$ .

Experimental data acquired for complex [**2b**]OTf displayed a rhombic  $^{15}\text{N}$  chemical shift tensor wherein the skew of the shielding tensor  $\kappa = 0.91$ . Since calculations performed on cation [**2b-m**] provided the expected axially symmetric spectrum it is difficult to identify the electronic features of complex [**2b**]OTf that contribute to the asymmetry of the experimental spectrum.

The lack of an axis of symmetry in the optimized geometry for model cation [**2c-m**] is immediately apparent from the calculated values of the chemical shift tensor for [**2c-m**] ( $\delta_{11(\text{calc})} = 695$  ppm,  $\delta_{22(\text{calc})} = 642$  ppm and  $\delta_{33(\text{calc})} = 183$  ppm). Our experimental results for complex [**2c**]OTf displayed greater asymmetry ( $\kappa = 0.16$ ) compared to the calculated spectrum ( $\kappa = 0.79$ ). Analysis of DFT calculations performed on cation [**2c-m**] shows that the principal contribution to  $\delta_{11(\text{calc})}$  is provided by mixing in the applied field of HOMO – 3,  $\sigma(\text{N } p_z\text{-C } p_z)$  with LUMO + 1,  $\pi^*(\text{Mo } d_{xz}\text{-N } p_x)$ . The principal contribution to  $\delta_{22(\text{calc})}$  is provided by mixing in the applied field of HOMO – 9,  $\pi(\text{Mo } d_{xz}\text{-N } p_x)$  with LUMO+2,  $\sigma^*(\text{N } p_z\text{-C } p_z)$ . For [**2c-m**] the  $\sigma(\text{N } p_z\text{-C } p_z)$  orbital is much higher in energy than the  $\sigma$ -orbital comprising the N–C bond in [**2a-m**] and [**2d-m**]. Indeed, the energy ordering of the frontier orbitals in [**2c-m**] is more reminiscent of that seen in the Lewis acid adducts (**1-LA**) than the other imido complexes. This implies that a weaker bonding interaction exists between the terminal N-atom and the electrophilic C-atom of the benzoyl fragment (compared to the interaction in other imido complexes) suggesting that resonance forms do not provide significant stabilization in complex [**2c**]OTf. These facts are consistent with the crystal structure of [**2c**]OTf in which the N–C single bond does not appear to be shortened through additional  $\pi$ -interactions.

#### 4.4. Theoretical studies on $\text{H}_2\text{CNMo}(\text{N}^i\text{Bu})\text{Ar}_3$ (**3**)

The overall sequence leading to ketimide **3** embodies formal carbene ( $\text{CH}_2$ ) addition to complex **1**, a process that encompasses C=N bond formation along with the reduction of molybdenum from the +6 to the +4 formal oxidation state.<sup>8</sup> Carbene addition to **1** is recognized as a potentially valuable means for the activation of complex **1** in the context of nitrogen atom transfer from  $\text{N}_2$  into organic molecules [91]. It was therefore of interest to determine what insight solid state NMR spectroscopy could provide, in conjunction with DFT analysis of the experimental shift tensors into the electronic

<sup>8</sup>  $\Delta H_{\text{RXN}}$  of  $\text{CH}_2$  addition to  $\text{NMo}(\text{NH}_2)_3$  is calculated to be  $-93$  kcal  $\text{mol}^{-1}$ .

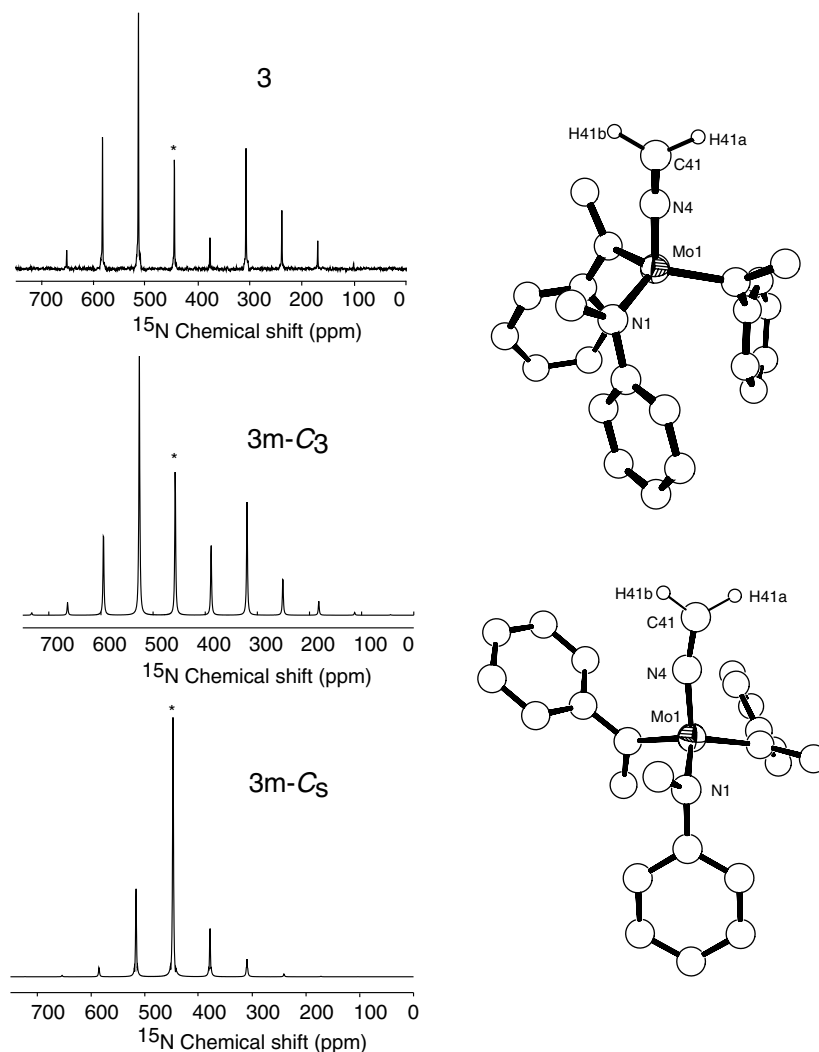


Fig. 9. Optimized geometries for the complexes **3m-C<sub>3</sub>** (top) and **3m-C<sub>5</sub>** (bottom) and solid state <sup>15</sup>N spectra for complex **3**: experimental (top), calculated **3m-C<sub>3</sub>** (middle) and calculated **3m-C<sub>5</sub>** (bottom). The isotropic peak is indicated by an asterisk.

structure at this N-atom which is activated toward productive removal from the molybdenum complex into an organic product.

Interestingly, attempts to use DFT to reproduce the observed <sup>15</sup>N solid state CP/MAS NMR spectrum of **3** using H<sub>2</sub>CNMo(NH<sub>2</sub>)<sub>3</sub>, (the structure of which converged to near C<sub>s</sub> symmetry) as the computational model were not entirely satisfactory. We probed further and found that the larger model H<sub>2</sub>CNMo(N[CH<sub>3</sub>]Ph)<sub>3</sub> (**3m**) converged either to a pseudo-C<sub>s</sub> (**3m-C<sub>s</sub>**) or to a pseudo-C<sub>3</sub> (**3m-C<sub>3</sub>**) conformation depending upon the initial geometry employed. The <sup>15</sup>N spectrum calculated for **3m-C<sub>3</sub>** was a good match to the observed spectrum of **3** ( $\chi^2 = 18$ ), while that calculated for **3m-C<sub>s</sub>** deviated noticeably ( $\chi^2 = 125$ ) (Fig. 9). The two local minima for **3m** differ with respect to rotation about the Mo–N<sub>amide</sub> bonds, leading to differing Mo–N<sub>amide</sub> d $\pi$ –p $\pi$  overlap, to which the ketimide nitrogen electronic environment is clearly sen-

sitive. Analyses of the NMR calculation performed on **3m-C<sub>3</sub>** reveals that the principal contributions to the most deshielded components of the tensor,  $\delta_{11(\text{calc})}$  and  $\delta_{22(\text{calc})}$  (600 and 563 ppm, respectively), result from mixing in the applied field of HOMO,  $\pi(\text{N-C})$  with LUMO,  $\pi^*(\text{Mo } d_{yz}-\text{N } p_y)$  and LUMO + 1,  $\pi^*(\text{Mo } d_{xz}-\text{N } p_x)$ . The same orbitals are responsible for the paramagnetic contributions to  $\delta_{11(\text{calc})}$  and  $\delta_{22(\text{calc})}$  in **3m-C<sub>s</sub>** ( $\delta_{11} = 570$  ppm,  $\delta_{22} = 457$  ppm) however, the energy gap ( $e_{\text{occ}} - e_{\text{vir}}$ ) between the HOMO and LUMO orbitals in **3m-C<sub>3</sub>** is appreciably smaller than in **3m-C<sub>s</sub>** (1.498 eV versus 1.696 eV). This increased energetic separation of the orbitals in **3m-C<sub>s</sub>** reduces the degree of magnetic coupling and results in a more shielded value of  $\delta_{11}$ .

In addition, the calculated molecular orbitals for **3m-C<sub>3</sub>** show significant p orbital contribution from the ketimide carbon to the HOMO. This indicates that the ketimide carbon has been rendered nucleophilic upon

dehydrohalogenation of the methylimido complex [2a]I. Experimental evidence for this is demonstrated by the reaction of **3** with CH<sub>3</sub>I to generate the ethylimido complex [2d]I.

## 5. Conclusions

The electronic structure of a dinitrogen-derived terminal molybdenum nitride complex  $\text{NMo}(\text{N}^{\text{t-Bu}}\text{Ar})_3$  (**1**) has been studied by the combined use of <sup>15</sup>N solid state CP/MAS NMR spectroscopy and DFT calculations. Parallels may be drawn between the bonding observed in this terminal nitride complex and the analogous terminal phosphide and carbide complexes. Perturbation of the electronic structure in the terminal molybdenum nitride complex (**1**) upon coordination of a Lewis acid can be attributed to stabilization of a  $\sigma$ -symmetric orbital as a result of N–LA bond formation.

Upon formation of a Lewis acid adduct of **1**, the increased energy gap ( $e_{\text{occ}} - e_{\text{vir}}$ ) between magnetically coupled occupied and virtual orbitals, is seen to correlate with a reduction in the magnitude of the perpendicular components of the chemical shift tensor ( $\delta_{11}$  and  $\delta_{22}$ ).

The reaction of **1** with electrophiles RX, results in further stabilization of the  $\sigma$ -symmetric orbital containing the N-lone pair of electrons. The paramagnetic contribution to the chemical shift tensor in this series of cationic imido complexes results from rotational mixing in the applied field of high-lying  $\pi(\text{Mo}-\text{N})$  orbitals with a low-lying  $\sigma(\text{N}-\text{E})$  (E = C, Si) orbital.

Finally, the strength of this combined approach to studying the electronic structure of spin-active nuclei in transition metal complexes is highlighted by our investigations into a ketimide complex,  $\text{H}_2\text{CNMo}(\text{N}^{\text{t-Bu}}\text{Ar})_3$  (**3**). Computational studies performed on the model complex  $\text{H}_2\text{CNMo}(\text{N}[\text{CH}_3]\text{Ph})_3$  (**3m**) identified two geometries to which this complex could converge. The variation in Mo–N  $d\pi$ – $p\pi$  overlap in the two structures is reflected in the calculated chemical shift tensors. A quantitative comparison of the experimental spectrum with the calculated spectra indicates that a closer match is provided by the pseudo- $C_3$  symmetric model, the optimized geometry of which is in good agreement with X-ray crystallographic data for complex **3**.

## Acknowledgements

For support of this work, we are grateful to the US National Science Foundation (CHE 0316823) and the National Institutes of Health (EB002026). Christopher Clough is thanked for his assistance with crystallography. We thank Dr. Christopher D. Incarvito for his crystallographic expertise in the structural refinement of complex **1**-SnCl<sub>2</sub>. N.M.L. thanks the National Institutes

of Health for support via a National Research Service Award post-doctoral fellowship (F32 NS42425-01).

The authors acknowledge the significant contributions made to inorganic and organometallic chemistry by Prof. Malcolm L.H. Green and the inspiration his work has provided to many of his colleagues during the course of his distinguished career.

## Appendix A. Supplementary material

Complete crystallographic data for complexes **1**-BF<sub>3</sub> (CCDC-236925), **1**-GeCl<sub>2</sub> (CCDC-236927), **1**-SnCl<sub>2</sub> (CCDC-236930), [2b]OTf (CCDC-236926), [2c]OTf (CCDC-236928), [2d]I (CCDC-236929) and **3** (CCDC-236924) have been deposited in the Cambridge Structural Database and can be obtained free of charge via [www.ccdc.cam.ac.uk/conts/retrieving.htm](http://www.ccdc.cam.ac.uk/conts/retrieving.htm) (or from the Cambridge Crystallographic Data Center, 12 Union Road, Cambridge CB21EZ, UK; (fax: +44-1223-336-033; or [deposit@ccdc.cam.ac.uk](mailto:deposit@ccdc.cam.ac.uk)). Supplementary Information for this article includes the following materials: ORTEP plots, anisotropic displacement parameters, atomic coordinates, bond lengths and angles for complexes **1**-BF<sub>3</sub>, **1**-GeCl<sub>2</sub>, **1**-SnCl<sub>2</sub>, [2b]OTf, [2c]OTf, [2d]I and **3**; details of DFT calculations including optimized geometries of all model complexes and selected (calculated) orbitals for complexes **1m**, **1m**-BCl<sub>3</sub>, [2b-m], [2c-m] and **3m**-C<sub>3</sub>; experimental information for the acquisition of solid state spectra; representative experimental, simulated and calculated solid state <sup>15</sup>N CP/MAS spectra. Supplementary data associated with this article can be found, in the online version at [doi:10.1016/j.poly.2004.08.010](https://doi.org/10.1016/j.poly.2004.08.010).

## References

- [1] D.D. Laws, H.-M.L. Bitter, A. Jerschow, *Angew. Chem., Int. Ed.* 41 (2002) 3096.
- [2] R.G. Griffin, *Nat. Struct. Biol.* 5 (1998) 508.
- [3] S.J. Opella, K.M. Morden, in: S.E. Harding, A.J. Rowe (Eds.), *Dynamic Properties of Biomolecular Assemblies*, The Royal Society of Chemistry, Cambridge, 1989, p. 196.
- [4] E.Y. Chekmenev, Q. Zhang, K.W. Waddell, M.S. Mashuta, R.J. Wittebort, *J. Am. Chem. Soc.* 126 (2004) 379.
- [5] S. Luca, H. Heise, M. Baldus, *Acc. Chem. Res.* 36 (2003) 858.
- [6] A. Shoji, S. Ando, S. Kuroki, I. Ando, G.A. Webb, *Structural studies of peptides and polypeptides in the solid state by nitrogen-15 NMR*, *Ann. Rep. NMR Spectrosc.* 26 (1993) 55.
- [7] C.P. Jaroniec, J. Lansing, B. Tounge, M. Belenky, J. Herzfeld, R.G. Griffin, *J. Am. Chem. Soc.* 123 (2001) 12929.
- [8] A.E. McDermott, T. Polenova, A. Bockmann, K.W. Zilm, G.T. Montellione, *J. Biomol. NMR* 16 (1999) 209219.
- [9] F. Castellani, B. van Rossum, A. Diehl, M. Schubert, K. Rehbein, H. Oschkinat, *Nature* 420 (2002) 98.
- [10] D.L. Bryce, R.E. Wasylshen, *Phys. Chem. Chem. Phys.* 4 (2002) 3591.
- [11] Y. Huang, D.F.R. Gilson, I.S. Butler, *J. Chem. Soc., Dalton Trans.* (1992) 2881.
- [12] R. Salzmann, M. Wojdelski, M. McMahon, R.H. Havlin, E. Oldfield, *J. Am. Chem. Soc.* 120 (1998) 1349.

- [13] G.M. Bernard, R.E. Wasylishen, *Phys. Organomet. Chem.* 3 (2002) 165.
- [14] R. Salzmann, C.J. Ziegler, N. Godbout, M.T. McMahon, K.S. Suslick, E. Oldfield, *J. Am. Chem. Soc.* 120 (1998) 11323.
- [15] N. Godbout, L.K. Sanders, R. Salzmann, R.H. Havlin, M. Wojdelski, E. Oldfield, *J. Am. Chem. Soc.* 121 (1999) 3829.
- [16] R. Gobetto, *Mater. Chem. Phys.* 29 (1991) 221.
- [17] M. Mehring, *Principals of High Resolution NMR in Solids*, 2nd ed., Springer-Verlag, Berlin, 1983.
- [18] M.J. Duer (Ed.), *Solid-state NMR: Principals and Applications*, Blackwell Science, Oxford, 2002.
- [19] G. Wu, D. Rovnyak, M.J.A. Johnson, N.C. Zanetti, D.G. Musaev, K. Morokuma, R.R. Schrock, R.G. Griffin, C.C. Cummins, *J. Am. Chem. Soc.* 118 (1996) 10654.
- [20] C.E. Laplaza, M.J.A. Johnson, J.C. Peters, A.L. Odom, E. Kim, C.C. Cummins, G.N. George, I.J. Pickering, *J. Am. Chem. Soc.* 118 (1996) 8623.
- [21] C.E. Laplaza, C.C. Cummins, *Science* 268 (1995) 861.
- [22] W. von Philipsborn, R. Müller, *Angew. Chem., Int. Ed.* 25 (1986) 383.
- [23] The ADF package utilized in this study allows the calculation of NMR shielding tensors: G. Schreckenbach, T. Ziegler, *J. Phys. Chem.* 99 (1995) 606.
- [24] G. Schreckenbach, T. Ziegler, *Int. J. Quantum Chem.* 60 (1996) 753.
- [25] G. Schreckenbach, T. Ziegler, *Int. J. Quantum Chem.* 61 (1997) 899.
- [26] S.K. Wolff, T. Ziegler, *J. Chem. Phys.* 109 (1998) 895.
- [27] G. Schreckenbach, T. Ziegler, *Theor. Chem. Acc.* 99 (1998) 71.
- [28] A.B. Pangborn, M.A. Giardello, R.H. Grubbs, R.K. Rosen, F.J. Timmers, *Organometallics* 15 (1996) 1518.
- [29] L. Brown, M. Koreeda, *J. Org. Chem.* 49 (1984) 3875.
- [30] D.D. Perrin, W.L.F. Armarego, *Purification of Laboratory Chemicals*, 3rd ed., Pergamon Press, Oxford, 1988.
- [31] Theoretical basis of the cross polarization experiment: S.R. Hartmann, E.L. Hahn, *Phys. Rev.* 128 (1962) 2042.
- [32] M.M. Maricq, J.S. Waugh, *J. Chem. Phys.* 70 (1979) 3300.
- [33] J. Herzfeld, A.E. Berger, *J. Chem. Phys.* 73 (1980) 6021.
- [34] M. Bak, J.T. Rasmussen, N.C. Nielsen, *J. Magn. Reson.* 147 (2000) 296.
- [35] E.J. Baerends, D.E. Ellis, P. Ros, *Chem. Phys.* 2 (1973) 41.
- [36] L. Versluis, T. Ziegler, *J. Chem. Phys.* 322 (1988) 88.
- [37] G. te Velde, E.J. Baerends, *J. Comput. Phys.* 99 (1992) 84.
- [38] C. Fonseca Guerra, J.G. Snijders, G. te Velde, E.J. Baerends, *Theor. Chem. Acc.* 99 (1998) 391.
- [39] J.G. Snijders, E.J. Baerends, P. Ros, *Mol. Phys.* 38 (1979) 1909.
- [40] T. Ziegler, V. Tschinke, E.J. Baerends, J.G. Snijders, W.J. Ravenek, *Phys. Chem.* 93 (1989) 3050.
- [41] E. van Lenthe, E.J. Baerends, J.G. Snijders, *J. Chem. Phys.* 99 (1993) 4597.
- [42] S.H. Vosko, L. Wilk, M. Nusair, *Can. J. Phys.* 58 (1980) 1200.
- [43] A.D. Becke, *Phys. Rev. A* 38 (1988) 3098.
- [44] J.P. Perdew, *Phys. Rev. B* 33 (1986) 8822.
- [45] G. Schreckenbach, T. Ziegler, *J. Phys. Chem.* 99 (1995) 606.
- [46] C. van Wüllen, *Phys. Chem. Chem. Phys.* 2 (2000) 2137.
- [47] W. Witkowski, W. Sicinska, G.A. Webb, *Spectroscopy* 9 (1991) 55.
- [48] C.J. Jameson, A.K. Jameson, D. Oppusunggu, S. Wille, P.M. Burrell, J. Mason, *J. Chem. Phys.* 74 (1981) 81.
- [49] Deuterated isotopomer synthesized by A.J. Johnson, Ph.D. Thesis, Massachusetts Institute of Technology, Cambridge, MA, 1997.
- [50] J.C. Peters, J.-P.F. Cherry, J.C. Thomas, L. Baraldo, D.J. Mindiola, W.M. Davis, C.C. Cummins, *J. Am. Chem. Soc.* 121 (1999) 10053.
- [51] Y.-C. Tsai, C.C. Cummins, *Inorg. Chim. Acta.* 345 (2003) 63.
- [52] J.F. Hinton, R.W. Briggs, in: B.E. Mann, R.K. Harris (Eds.), *NMR and the Periodic Table*, Academic Press, London, 1978, Chapter 9,  $^{27}\text{Al}$  NMR (reference  $[\text{Al}(\text{D}_2\text{O})_6]^{3+}$ , 0.0 ppm)  $\text{Al}_2\text{Cl}_6$  (2 M,  $\text{Et}_2\text{O}$ )  $\delta$ 105 ppm;  $\text{Al}_2\text{Br}_6$  (1.5 M,  $\text{Et}_2\text{O}$ )  $\delta$ 95 ppm;  $\text{Al}_2\text{I}_6$  (1.5 M,  $\text{Et}_2\text{O}$ )  $\delta$ 40 ppm.
- [53] P.C. Lauterbur, J.J. Burke, *J. Am. Chem. Soc.* 83 (1961) 326.
- [54] C.C. Hsu, R.A. Geanangel, *Inorg. Chem.* 19 (1980) 110.
- [55] L.H. Doerrer, A.J. Graham, M.L.H. Green, *J. Chem. Soc., Dalton Trans.* (1998) 3941.
- [56] R. Dantona, E. Schweda, J. Strähle, *Z. Naturforsch. B* 39 (1984) 733.
- [57] U. Abram, B. Schmidt-Brücken, A. Hagenbach, M. Hecht, R. Kirmse, A. Voigt, *Z. Anorg. Allg. Chem.* 629 (2003) 838.
- [58] Tin halide adducts with N-donor molecules: J.D. Donaldson, D.G. Nicholson, *Inorg. Nuc. Chem. Lett.* 6 (1970) 151.
- [59] W.W. Du Mont, H.J. Kroth, *Naturforsch. B* 35 (1980) 700.
- [60] W.A. Nugent, J.M. Mayer, *Metal-Ligand Multiple Bonds*, Wiley, New York, 1988.
- [61] R.A. Eikey, M.M. Abu-Omar, *Coord. Chem. Rev.* 243 (2003) 83, and references therein.
- [62] N-Si single bond distances are typically ca. 1.711 Å: D.R. Lide (Ed.), *CRC Handbook of Chemistry and Physics*, 86th ed., CRC Press, London, 2003, p. 9.
- [63] F. Effenberger, E. Sohn, G. Epple, *Chem. Ber.* 116 (1983) 1195.
- [64] Dissociation tendency of benzoyl triflate: F. Effenberger, G. Epple, J.K. Eberhard, U. Buehler, E. Sohn, *Chem. Ber.* 116 (1983) 1183.
- [65] D.E. Wigley, *Prog. Inorg. Chem.* 42 (1994) 239.
- [66] A.J. Nielson, P.A. Hunt, C.E.F. Rickard, P. Schwerdtfeger, *J. Chem. Soc., Dalton Trans.* (1997) 3311.
- [67] C. Tong, L.A. Bottomley, *J. Porphyrins Phthalocyanines* 2 (1998) 261.
- [68] C.R. Clough, J.B. Greco, J.S. Figueroa, P.L. Diaconescu, W.M. Davis, C.C. Cummins, *J. Am. Chem. Soc.* 126 (2004) 7742.
- [69] N.C. Mösch-Zanetti, R.R. Schrock, W.M. Davis, K. Wanninger, W.S. Seidel, M.B. O'Donoghue, *J. Am. Chem. Soc.* 119 (1997) 11037.
- [70] P.A. Shapley, J.M. Shusta, J.L. Hunt, *Organometallics* 15 (1996) 1622.
- [71] A. Hills, D.L. Hughes, C.J. Macdonald, M.Y. Mohammed, C.J. Pickett, *J. Chem. Soc., Dalton Trans.* (1991) 121.
- [72] J. Chatt, R.J. Dosser, G.J. Leigh, *Chem. Commun.* (1972) 1243.
- [73] N.N. Greenwood, A. Earnshaw, *Chemistry of the Elements*, 2nd ed., Butterworth-Heinemann, Oxford, 1998, p. 375.
- [74] Ketimines undergo reactions with organolithium reagents ( $\text{R}'\text{Li}$ ) to form  $\text{R}(\text{Li})\text{N}-\text{C}(\text{R}')\text{H}_2$  via addition of nucleophilic  $[\text{R}'^-]$  to the electrophilic carbon of the ketimine: J. Huet, *Bull. Soc. Chim. Fr.* (1964) 952, p. 960, 967 and 973.
- [75] M.B. Smith, J. March, *March's Advanced Organic Chemistry*, 5th ed., Wiley, New York, 2001, p. 431.
- [76] Conventions followed in this paper are defined in the following article: J. Mason, *Solid State Nucl. Magn. Reson.* 2 (1993) 285.
- [77] Polymorphism and characterization by solid state NMR spectroscopy: M. Strohmeier, A.M. Orendt, D.W. Alderman, D.M. Grant, *J. Am. Chem. Soc.* 123 (2001) 1713.
- [78] M.T. Zell, B.E. Padden, D.J. Grant, M.-C. Chapeau, I. Prakash, E.J. Munson, *J. Am. Chem. Soc.* 121 (1999) 1372.
- [79] J. Smith, E. MacNamara, D. Rafferty, T. Borchardt, S. Byrn, *J. Am. Chem. Soc.* 120 (1998) 11710.
- [80] Q. Cui, D.G. Musaev, M. Svensson, S. Sieber, K. Morokuma, *J. Am. Chem. Soc.* 117 (1995) 12366.
- [81] K.M. Neyman, V.A. Nasluzov, J. Hahn, C.R. Landis, N. Rösch, *Organometallics* 16 (1997) 995.
- [82] C.J. Jameson, J. Mason, in: J. Mason (Ed.), *Multinuclear NMR*, Plenum Press, New York, 1987, p. 51.
- [83] G. Schreckenbach, *J. Chem. Phys.* 110 (1999) 11936.
- [84] Y. Ruiz-Morales, T. Ziegler, *J. Phys. Chem. A* 102 (1998) 3970.
- [85] Y. Ruiz-Morales, G. Schreckenbach, T. Ziegler, *J. Phys. Chem. A* 101 (1997) 4121.

- [86] Y. Ruiz-Morales, G. Schreckenbach, T. Ziegler, *Organometallics* 15 (1996) 3920.
- [87] Y. Ruiz-Morales, G. Schreckenbach, T. Ziegler, *J. Phys. Chem.* 100 (1996) 3359.
- [88] G. Schreckenbach, Y. Ruiz-Morales, T. Ziegler, *J. Chem. Phys.* 104 (1996) 8605.
- [89] A.W. Ehlers, Y. Ruiz-Morales, E.J. Baerends, T. Ziegler, *Inorg. Chem.* 36 (1997) 5031.
- [90] J.B. Greco, J.C. Peters, T.A. Baker, W.M. Davis, C.C. Cummins, G. Wu, *J. Am. Chem. Soc.* 123 (2001) 5003.
- [91] H. Henderickx, G. Kwakkenbos, A. Peters, J. van der Spoel, K. de Vries, *Chem. Commun.* 16 (2003) 2050.